

Development of LC-MS/MS-Based Receptor Occupancy Tracers and Positron Emission Tomography Radioligands for the Nociceptin/Orphanin FQ (NOP) Receptor

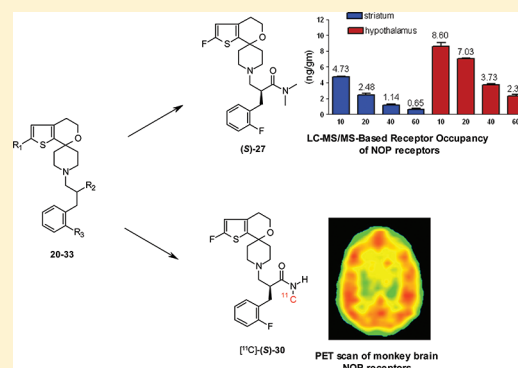
Concepción Pedregal,^{*,†} Elizabeth M. Joshi,[‡] Miguel A. Toledo,[†] Celia Lafuente,[†] Nuria Diaz,[†] Maria A. Martinez-Grau,[†] Alma Jiménez,[†] Ana Benito,[†] Antonio Navarro,[‡] Zhaogen Chen,[‡] Daniel R. Mudra,[‡] Steven D. Kahl,[‡] Karen S. Rash,[‡] Michael A. Statnick,[‡] and Vanessa N. Barth^{*,‡}

[†]Centro de Investigación Lilly, Avenida de la Industria 30, 28108-Alcobendas, Madrid, Spain

[‡]Eli Lilly & Co., Lilly Research Laboratories, Indianapolis, Indiana 46285, United States

S Supporting Information

ABSTRACT: Currently, a lack of sufficient tools has limited the understanding of the relationship between neuropsychiatric disorders and the nociceptin/orphanin FQ (N/OFQ) peptide (NOP) receptor. Herein, we describe the discovery and development of an antagonist NOP receptor occupancy (RO) tracer and a novel positron emission tomography (PET) radioligand suitable to probe the NOP receptor in human clinical studies. A thorough structure–activity relationship (SAR) around the high-affinity 3-(2'-fluoro-4',5'-dihydrospiro[piperidine-4,7'-thieno[2,3-*c*]pyran]-1-yl)-2-(2-halobenzyl)-*N*-alkylpropanamide scaffold identified a series of subnanomolar, highly selective NOP antagonists. Subsequently, these unlabeled NOP ligands were evaluated *in vivo* by liquid chromatography–tandem mass spectrometry (LC-MS/MS) in rat to determine brain uptake, kinetics and specific binding. (S)-27 was identified as a suitable unlabeled preclinical RO tracer to accurately quantify NOP receptor engagement in rat brain. Three compounds were selected for evaluation in nonhuman primates as PET tracers: (–)-26, (–)-30, and (–)-33. Carbon-11 labeling of (+)-31 yielded [¹¹C]-(S)-30, which exhibited minimal generation of central nervous system (CNS) penetrant radiometabolites, improved brain uptake, and was an excellent PET radioligand in both rat and monkey. Currently [¹¹C]-(S)-30 is being evaluated as a PET radiotracer for the NOP receptor in human subjects.



■ INTRODUCTION

Nociceptin/orphanin FQ^{1,2} (N/OFQ) is a 17 amino acid peptide and was the first neuropeptide discovered by screening the orphan G protein-coupled receptor LC132 using fractionated brain extracts. The receptor for N/OFQ is the opioid receptor-like 1 (ORL1) or nociceptin opioid peptide (NOP) receptor, a class A GPCR that is widely expressed in the central nervous system (CNS). ORL1/NOP receptors are also expressed in the peripheral nervous system, gastrointestinal tract, smooth muscle, and immune system. NOP receptors are coupled to the cAMP cascade as well as to voltage-gated Ca²⁺ and K⁺ channels.³ While N/OFQ is similar to opioid peptides, it exhibits no significant cross reactivity at the classical opioid receptors μ , κ , and δ . Moreover, the classical opioid peptides (enkephalins, endorphin, and dynorphin) do not bind to ORL1/NOP receptors. *In vivo*, N/OFQ modulates several physiological functions and behaviors in animal models including depression, stress, anxiety, feeding, locomotor activity, body temperature, substance abuse, memory, and pain.^{4–6} Accordingly, the brain NOP receptor is a target of interest to study physiological mechanisms of CNS function and is also a potential target for the discovery of novel drug therapies.⁴

Positron emission tomography (PET)⁷ is a powerful non-invasive *in vivo* imaging technique that measures radiolabeled molecules permitting measurements of receptor occupancy (RO), target expression, and provides indirect pharmacodynamic measures such as endogenous transmitter tone. Molecular imaging affords data that can aid in selecting drug candidates, identifying optimal dosing regimens, and validating targets. However, investigation of these opportunities is predicated on having the tool, or tracer, available to do so. The development of PET tracers is challenging in the context of balancing physicochemical properties to achieve specific target binding (reduced nonspecific binding), suitable brain uptake/penetration, and appropriate brain and plasma kinetics, while maintaining *in vivo* activity, selectivity, and avoiding radiometabolite interference.^{8–11}

In vivo RO can be calculated based on blockade of the target specific binding of the tracer, as is the case with PET and single photon emission computed tomography (SPECT) occupancy studies. The use of the high performance liquid chromatography

Received: August 11, 2011

Published: April 30, 2012

coupled to tandem mass spectrometry (LC-MS/MS) method to conduct in vivo target occupancy experiments has a number of advantages, the most obvious being avoidance of the environmental, regulatory, and purchase costs of working with radiopharmaceuticals. In addition, use of LC-MS/MS permits one the ability to run target engagement experiments more quickly, achieving high-throughput in vivo screening, the ability to establish occupancy-exposure relationships by measuring the test compound along with the tracer within the same animal, and the ability to use multiple tracers in the same animal to evaluate receptor selectivity. Most importantly, the LC-MS/MS evaluation of unlabeled molecules after intravenous microdosing enables the evaluation of new potential tracers much faster than is feasible using traditional radiolabeled screening paradigms.^{12,13}

Finding tracers for new targets is the rate limiting step in generating both preclinical unlabeled target occupancy assays as well as for PET/SPECT imaging of those targets. Because few small molecules possess the physicochemical properties of a good tracer (i.e., high potency, high selectivity, high brain uptake, and the ability to differentially distribute between target rich and target poor tissues), one typically needs to examine many candidate molecules. Instead of the weeks to months required to label and test a new tracer using traditional radiolabeled techniques, a unlabeled tracer candidate can be tested in a day using the LC-MS/MS methodology. Employing LC-MS/MS evaluation of unlabeled tracer candidates permits increased iterations and learning within the structure–activity relationship (SAR) and expands the chemical space to include molecules without labeling sites or with challenging labeling chemistry. The desirable properties for a candidate unlabeled LC-MS/MS tracer include high binding affinity and selectivity for the receptor and low nonspecific binding. Tracers enabling LC-MS/MS based RO assays do not require a label site, nor do they require as high a brain uptake, or standardized uptake value (SUV), that a PET tracer requires. Radiometabolites are not generated because only the parent tracer molecule is measured by LC-MS/MS, eliminating a significant source of interference. Removal of both active and inactive radiometabolites increase the chance of seeing a differential distribution and identification of a chemical starting point for tracer discovery. Thus, using our LC-MS/MS methods, it is easier to identify a tracer suitable for preclinical studies. More often, than not, the identification of such a tool represents a starting point to design an optimized PET tracer suitable for clinical investigation. Throughout the entire tracer discovery process, the identification of a compound with low enough nonspecific binding to see a differential distribution toward a receptor rich tissue, versus a tissue devoid of or containing very little, target occurs earlier. Once a tracer is identified, investigators can use the RO data for dose selection in more labor intensive behavioral and neurochemical assays. In parallel, the development and optimization process for the PET tracer can be initiated.

Herein, we describe the discovery of a new series of high-affinity small molecules based on a dihydrospiro[piperidine-4,7'-thieno[2,3-*c*]pyrane] scaffold (**5**) (Chart 2) as unlabeled tracers for the NOP receptor. The identification of this scaffold has enabled the development of a preclinical receptor occupancy assay to prioritize SAR development. Furthermore, optimization of the preclinical tracer scaffold was undertaken to improve SUV and to mitigate against potential CNS penetrant radiometabolites. These efforts have led to the discovery of a successful nonhuman primate PET ¹¹C-labeled radioligand (2*S*)-[(2-fluorophenyl)methyl]-3-(2-fluorospiro[4,5-dihydrothieno[2,3-*c*]pyran-7,4'-piperidine]-

1'-yl)-*N*-methylpropanamide ([¹¹C]-(*S*)-**30**),^{14,15} which is currently under evaluation in human subjects.

RESULTS AND DISCUSSION

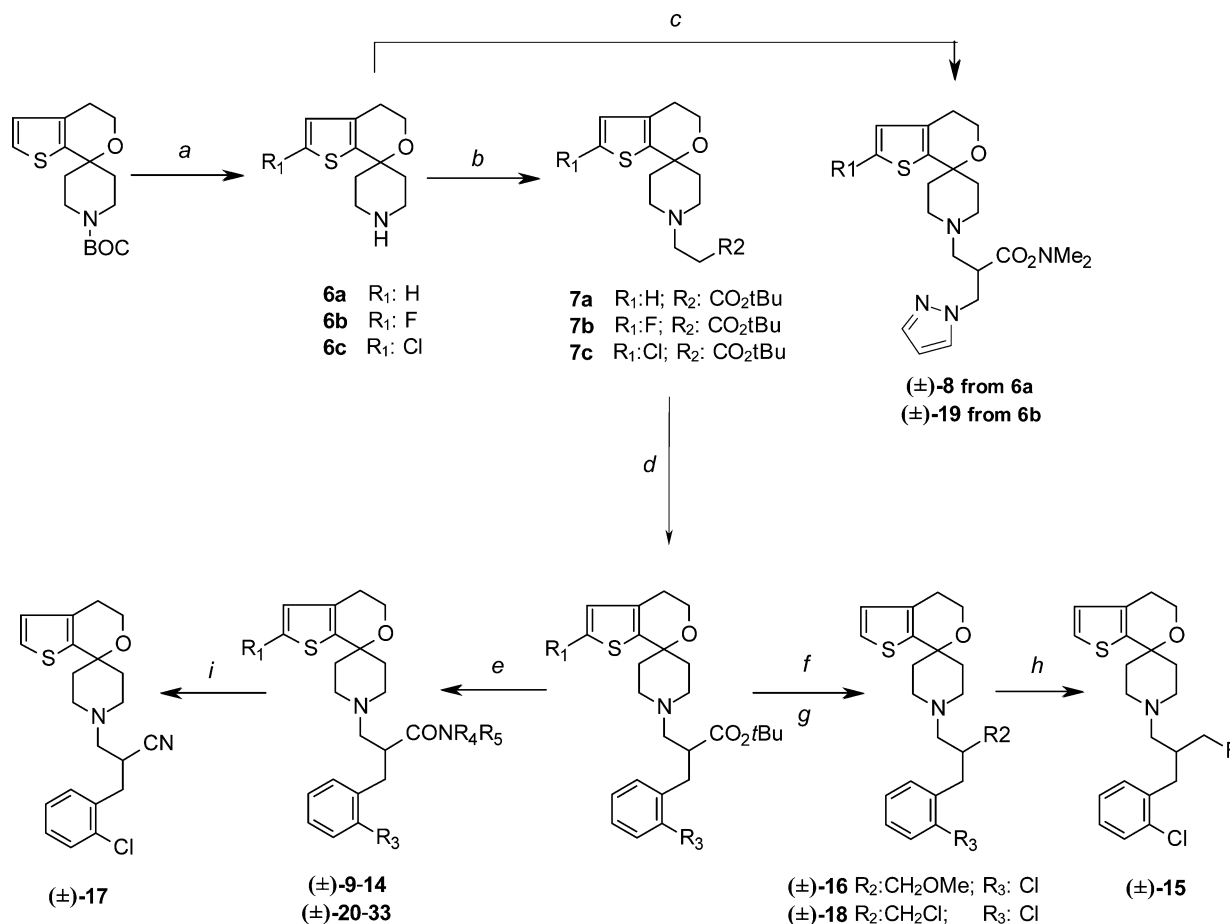
Chemistry. The synthetic route for generation of NOP ligands is outlined in Scheme 1. The synthesis of spiro[4,5-dihydrothieno[2,3-*c*]pyran-7,4'-piperidine] (**6a**) and 2-fluorospiro[4,5-dihydrothieno[2,3-*c*]pyran-7,4'-piperidine] (**6b**) is described in ref 14. Excellent yield of 2-chlorospiro[4,5-dihydrothieno[2,3-*c*]pyran-7,4'-piperidine] (**6c**) was obtained by chlorination of *N*-*tert*-butoxycarbonyl (BOC) protected piperidine **6a** with *N*-chlorosuccinimide followed by *N*-deprotection. Michael addition between the piperidine intermediates **6a–6c** and *tert*-butyl acrylate in the presence of triethylamine (TEA) yielded the common propanoate intermediates **7a–7c**. α -Alkylation of the propanoates **7a–7c** with the corresponding substituted benzyl bromides was achieved with LiN(TMS)₂ as base. Ester hydrolysis followed by conventional amide formation with the appropriate amine yielded the final racemic amides **9–14** and **20–33**. Racemic amides **10** and **20–33** were separated into individual enantiomers by chiral HPLC. The *L*-tartaric acid salt was prepared when the final compound was an oil.

In the same way, Michael addition of the piperidine intermediates **6a** and **6b** to ethyl 2-((1*H*-pyrazol-1-yl)methyl)acrylate gave rise to the corresponding Michael adducts. Ester hydrolysis under basic conditions followed by amide formation with dimethylamine hydrochloride afforded the final racemic amides (\pm)-**8** and (\pm)-**19**. Chiral chromatography was used to isolate single enantiomers.

Reduction of the *tert*-butyl esters with lithium aluminum hydride yielded the corresponding free alcohol. The alcohol was converted under basic conditions to the methyl ether compound (\pm)-**16** by treatment with dimethylsulfate. Alternatively, methanesulfonyl chloride was used in the transformation of the alcohol into the chlorinated product (\pm)-**18**. The fluorinated derivative (\pm)-**15** was synthesized from (\pm)-**18** following addition of *N*-tetrabutylammonium fluoride. Finally, the nitrile (\pm)-**17** was obtained by dehydration of the corresponding primary carboxamide.

Tracer Evaluation of Known NOP Ligands. The distribution of NOP receptors in rat brain has been studied by receptor binding autoradiography using peptide radioligands.^{16–19} In the rat brain, NOP binding sites are widely distributed throughout the neural axis. A relatively high density of NOP binding sites is present in the rat cortex, hypothalamus, thalamus, and amygdala, while low levels of NOP binding were found in the caudate putamen.^{16,17} The estimated density of NOP receptors in rat brain membranes is 237 fmol/mg protein (about 24 nM in whole brain assuming 100 mg protein per mL of tissue).¹⁷ Data on the distribution and density of NOP receptors in the brain of higher species are sparse except for a single study in macaque.²⁰ In macaques, the distribution of NOP was similar to that of the rat but with some notable differences, particularly in the straitum. In nonhuman primate, a NOP B_{\max} of greater than 6 fmol/mg of tissue (equating to >6 nM in whole brain) was found in NOP receptor-rich regions.

Using our LC-MS/MS methodology, specific binding is expressed as the binding potential (BP) and is defined as the ratio of the tracer concentration in a brain area with high receptor density divided by the tracer concentration detected in an area with little to no receptor expression, minus one. Additionally, brain uptake or standard uptake value (SUV) is calculated as the ratio of the tissue tracer levels divided by the

Scheme 1. Synthesis of NOP Carboxamides 8–14, 19–33, and Non-carboxamides Ligands 15–18^a

^aReagents and conditions: (a) For the synthesis of **6a** and **6b**, see ref 14. For **6c**: (1) NCS, CH₃CN, 70 °C, (2) 4 M HCl in dioxane, CH₂Cl₂, rt. (b) For the synthesis of **7b**, see ref 14. For **7a** and **7c**: *t*-butyl acrylate, TEA, THF, reflux. (c) (1) Ethyl 2-((1*H*)-pyrazol-1-ylmethyl) acrylate, TEA, MeOH, 68 °C, (2) LiOH/THF, (3) EDCl, HOBt, DIPEA, CH₂Cl₂, and HNMe₂·HCl. (d) (1) 1 M LiN(TMS)₂, THF, 1,3-dimethyl-tetrahydropyrimidin-2(1*H*)-one, THF, -78 °C, (2) 2-*R*₃-benzyl bromide. (e) For compounds **9–14** and compounds **20–33**: (1) TFA/CH₂Cl₂, rt, (2) EDCl, HOBt, DIPEA, CH₂Cl₂, and amine HNR₄R₅. (f) LiAlH₄, THF, reflux. (g) For compound **16**: (1) NaH, THF, 0 °C, (2) dimethyl sulfate, rt. For compound **18**: (1) TEA, CH₂Cl₂, 0 °C, (2) methanesulfonyl chloride, rt. (h) For compound **18**: *N*-tetrabutylammonium fluoride, THF, reflux. (i) For corresponding primary amide (R₄ and R₅:H): POCl₃, K₂CO₃, reflux.

injected tracer dose. Binding potential is mathematically defined as the B_{\max}/K_d and can be modeled or directly determined through PET/SPECT imaging studies. A guideline for tracer screening in vitro is that the product of receptor density (B_{\max} , nM) and ligand affinity ($1/K_d$, nM⁻¹) should exceed a value of 5 in target-rich regions of brain of interest (eq 1). As one can see from eq 1, tracer identification becomes more difficult for receptors expressed at low density in the tissue of interest.

$$B_{\max}/K_d > 5 \quad (1)$$

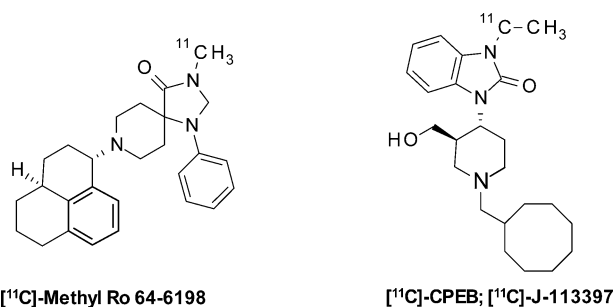
Therefore, with an estimated B_{\max} in rat brain of approximately 200 fmol/mg of tissue for NOP binding sites, we hypothesized that NOP RO tracer candidates should have a K_d value in the low nanomolar to subnanomolar range. By using these criteria, we have successfully identified several novel LC-MS/MS tracers that were optimized to generate PET ligands.^{21,22}

Two nonpeptide imaging agents have been previously reported for the NOP receptor: the agonist 8-[(1*S*,3*aS*)-2,3,3*a*,4,5,6-hexahydro-1*H*-phenalen-1-yl]-2-methyl-4-phenyl-2,4,8-triazaspiro[4.5]decan-1-one ([¹¹C]-methyl Ro 64–6198)²³ by Hoffmann-La Roche and the antagonist 1-[(3*R*,4*R*)-1-cyclo-

octyl-3-hydroxymethyl-4-piperidy]-3-[¹¹C]ethyl-1,3-dihydro-2*H*-benzimidazol-2-one ([¹¹C]-CPEB)²⁴ by Merck (Chart 1). We prepared the respective unlabeled analogues and demonstrated high affinity binding for the NOP receptor as well as high selectivity versus the classical μ , κ , and δ opioid receptors as reported (Table 1), however, neither compound was suitable as a tracer because of the high level of nonspecific binding reported.^{23,24}

NOP tracer identification was initiated by applying our previously published in vivo/ex vivo LC-MS/MS method^{12,13} to evaluate known small molecule NOP ligand agonists **1** (W-212393),²⁵ **2** (NNC 63–0532),²⁶ and the antagonist **3** (SB-612111)²⁷ as potential unlabeled RO tracers in rat (Chart 2).

While differences in receptor binding interactions between agonist and antagonist ligands exist, we were interested in evaluating compounds for their ability to behave as tracers, regardless of functional activity, because they are ligands with known affinity for the NOP receptor and exhibit CNS activity following systemic administration. The opioid receptor binding affinities and functional activities for **1**, **2**, and **3** can be found in Table 1. Consistent with previous reports, we found all three compounds were potent ligands at the NOP receptor while

Chart 1. Structure of [¹¹C]-Methyl Ro 64-6198 and [¹¹C]-CPEB

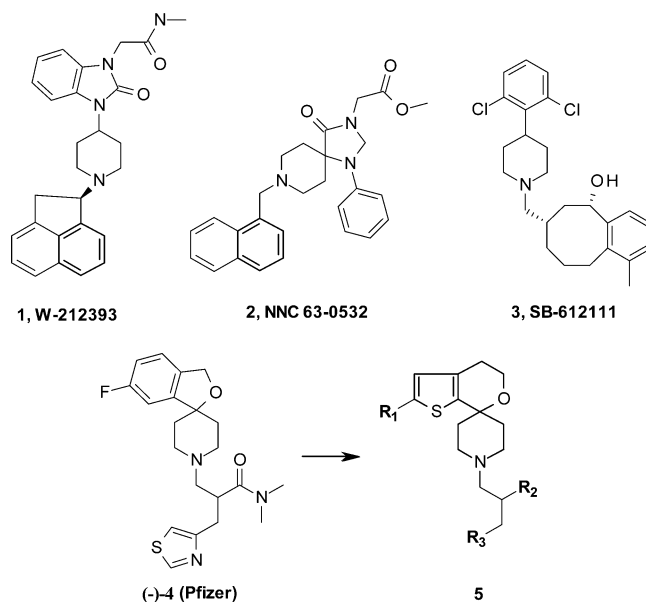
exhibiting high selectivity versus the classical μ , κ , and δ opioid receptors. We tested these molecules in vivo in rat by LC-MS/MS to establish any ability to differentially distribute between NOP receptor rich and poor brain regions. The first molecule evaluated, **1**, showed no SUV or BP due to high nonspecific binding (Table 2). Despite its lower affinity, **2** exhibited differential distribution between the NOP receptor rich region, hypothalamus, as compared to the striatum (a region with low NOP binding), giving BP = 3. However, **2** showed low brain uptake (SUV = 6%), preventing its use as a suitable LC-MS/MS tracer. On the contrary, **3** was found to have a significantly higher brain uptake (SUV = 130%), suggesting suitable penetration of the blood–brain barrier (BBB), but exhibited a low BP (0). Because of the measurable BP exhibited by **2**, this compound was subsequently studied as a tracer via blocking experiments with the antagonist **3**. No reduction in brain concentrations of **2** were observed following pretreatment with **3** in the hypothalamus, indicating that the differential distribution was likely due to nonspecific binding and was not attributed to specific binding of the NOP receptor. No additional studies were performed using **2**.

Next, we prepared the racemate 2-[(5-fluorospiro [1*H*-isobenzofuran-3,4'-piperidine]-1'-yl)methyl]-*N,N*-dimethyl-3-thiazol-4-yl-propanamide ((\pm)-**4**) described in patent WO 05092858 (Chart 2).²⁸ Following chiral chromatography of (\pm)-**4**, the active enantiomer was identified as (-)-**4**. Although less potent than the other antagonist molecules tested, (-)-**4** exhibited a measurable BP (1.3) and SUV (25%) (Table 2). Next, we explored substitution of the 5-fluorospiro[1*H*-isobenzofuran-3,4'-piperidine] piece of compound (-)-**4** with the spiro[4,5-dihydrothieno[2,3-*c*]pyran-7,4'-piperidine] motif and improved BP and SUV was retained as exemplified by compound (+)-**19**. Subsequently, we initiated an SAR study to optimize this novel NOP tracer scaffold.

Table 1. Opioid Receptor Binding Affinities and Functional Activities of the Known Enantiomerically Pure NOP Ligands Shown in Charts 1 and 2

ligand	NOP binding ^a K_i (nM)	NOP agonist ^a EC_{50} (nM)	NOP ^a % efficacy	NOP antagonist ^a K_b (nM)
Ro 64-6198 ^b	1.12 (0.251 $n = 3$)	21.0 (3.82 $n = 2$)	122	
CPEB (J-113397) ^b	0.403 (0.251 $n = 2$)			0.565 (0.0214 $n = 11$)
1 ^b	0.336 (0.155 $n = 2$)	1.60 (0.82 $n = 2$)	129	
2 ^b	12.9 (2.02 $n = 2$)	121 (20.02 $n = 2$)	103	
3 ^b	0.253 (0.087 $n = 3$)			0.258 (0.0743 $n = 3$)
(-)- 4 ^b	1.64 (0.647 $n = 3$)			1.22 (0.414 $n = 3$)

^aShown are geometric means (SEM, n) for K_i and K_b values. [³H]-Nociceptin was used as reference NOP radioligand in a binding assay using human recombinant NOP receptors expressed in CHO cells. Functional activity was determined in an assay of receptor-mediated G-protein activation using [³⁵S]-GTP γ S and membranes expressing cloned human NOP receptors. See Methods for assay details. ^bRadioligand binding with [³H]-diprenorphine, using membranes from CHO cells expressing human κ , μ , or δ opioid receptors gave K_i higher than 400 nM.

Chart 2. Structure of Known NOP Agonists: **1 (W-212393), **2** (NNC 63-0532), and Antagonists **3** (SB-612111), Pfizer compound (-)-**4**, and Novel Dihydrospiro[piperidine-4,7'-thieno[2,3-*c*]pyrane] Scaffold **5******Table 2. Comparison of LC-MS/MS Evaluation of BP, Brain Uptake (SUV), and Lipophilicity (Calculated and Measured) for the Known Enantiomerically Pure NOP Ligands Shown in Charts 1 and 2**

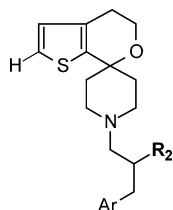
ligand	BP ^a	SUV ^b (%)	clogD ^c	log D^d
Ro 64-6198			4.05	3.46
CPEB (J-113397)			3.27	3.36
1	0	0	3.61	
2	3	6	2.88	3.85
3	0	130	4.97	3.56
(-)- 4	1.3	25	1.68	2.02

^a(BP) ratio of concentration of tracer in a hypothalamus versus striatum minus one. ^b(SUV) ratio of the concentration of the tracer in tissue to the injected tracer dose. ^cComputed with Pallas software. ^dlog D measured by the potentiometric method.

Ligand Pharmacology. Tables 3 and 4 contain compounds which were prepared for tracer evaluation with binding affinities and functional antagonism for the NOP receptor. We began the SAR by increasing the lipophilicity of the compounds by replacement of the pyrazyl heterocycle with a phenyl ring in

an effort to increase the permeability and subsequent brain uptake of the compounds into the CNS. Fortunately, we were able to maintain high affinity binding following phenyl ring substitution ((±)-8 versus (±)-9, Table 3). In addition, further

Table 3. Opioid Receptor Binding Affinities and Functional Activities of the Novel NOP Antagonists 8–18



ligand	R ₂	Ar	NOP binding ^a K _i (nM)	NOP antagonist ^a K _b (nM)
(±)-8 ^b	CONMe ₂	1-pyrazyl	7.37 (2.41 n = 2)	7.62 (1.93 n = 2)
(+)-8 ^c	CONMe ₂	1-pyrazyl	403 (47.5 n = 2)	>70
(-)-8 ^c	CONMe ₂	1-pyrazyl	2.05 (0.853 n = 3)	2.05 (0.353 n = 3)
(±)-9	CONMe ₂	phenyl	9.40 (0.345 n = 2)	4.12 (1.80 n = 2)
(±)-10 ^b	CONMe ₂	2-Cl-phenyl	1.84 (0.181 n = 2)	1.48 (0.921 n = 2)
(+)-10 ^c	CONMe ₂	2-Cl-phenyl	219 (40.34 n = 2)	129 (23.80 n = 2)
(-)-10 ^c	CONMe ₂	2-Cl-phenyl	0.458 (0.140 n = 3)	0.558 (0.099 n = 3)
(±)-11 ^b	CONMe ₂	2-F-phenyl	5.16 (0.804 n = 2)	1.71 (1.15 n = 2)
(±)-12 ^b	CONMe ₂	2,6-di-F-phenyl	>10	>10
(±)-13	CONMe ₂	2-Py	>10	>10
(±)-14	CONMe ₂	2-OMe-phenyl	>10	>10
(±)-15	CH ₂ -F	2-Cl-phenyl	>10	>10
(±)-16	CH ₂ -OMe	2-Cl-phenyl	>40	>40
(±)-17	CN	2-Cl-phenyl	>40	>40
(±)-18	CH ₂ -Cl	2-Cl-phenyl	>40	>40

^aShown are geometric means (SEM, *n*) for K_i and K_b values. [³H]-Nociceptin was used as reference NOP radioligand in a binding assay using human recombinant NOP receptors expressed in CHO cells. Antagonist activity was determined in an assay of receptor-mediated G-protein activation using [³⁵S]-GTPγS and membranes expressing cloned human NOP receptors. See methods for assay details.

^bRadioligand binding with [³H]-diprenorphine, using membranes from CHO cells expressing human κ, μ, or δ opioid receptors gave K_i higher than 400 nM. ^cL-Tartaric acid salt.

increase of lipophilicity by incorporation of a chlorine atom in the ortho position of the phenyl ring increased the affinity 5-fold (compare (±)-9 with (±)-10). Introduction of one fluorine atom in the ortho position ((±)-11) also maintained the affinity as compared to the chloro substitution. Meanwhile, the 2,6-difluorophenyl ((±)-12), the 2-pyridine ((±)-13), and methoxy derivatives ((±)-14) exhibited a significant reduction in affinity (K_i higher than 10 nM). Additionally, the influence of the carboxamide on receptor affinity was evaluated by replacing this group by fluoromethyl ((±)-15), methoxymethyl ((±)-16), nitrile ((±)-17), and chloromethyl ((±)-18). However, substitution of the carboxamide group resulted in considerable loss of affinity (K_i higher than 10 for (±)-15 and 40 nM for (±)-16–(±)-18). Thus, the racemic (±)-10 exhibited the highest affinity in this early phase of the SAR exploration while maintaining physicochemical properties

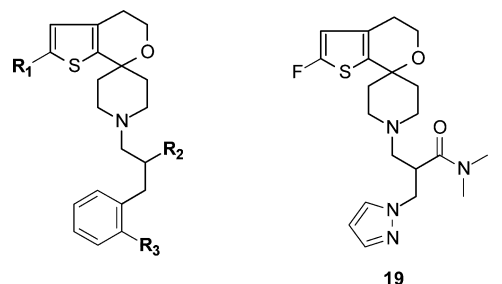
associated with good brain uptake. Asymmetric chiral chromatography was used to separate the individual enantiomers of (±)-8 and (±)-10, resulting in the identification of (-)-10 as the first subnanomolar molecule in the series. The affinity of the (+) enantiomers was significantly less potent, therefore, the high binding affinity of the racemates (±)-8 and (±)-10 resided exclusively in the (-) enantiomer (Table 3).

Next, to further explore the SAR in this scaffold, a chlorine or fluorine atom was introduced at the 2-position of the thiophenyl ring of the spiro system (Table 4 where data is shown for the most active enantiomer in most cases). This modification was shown to dramatically increase (around 10-fold) the affinity of (+)-19 in Table 4 versus (-)-8 in Table 3 and to a lesser extent (around 3-fold) in (-)-20 and (+)-25 in Table 4 versus (-)-10 in Table 3. A wide range of substituted carboxamides (primary, secondary, and tertiary) were also synthesized and found to maintain high affinity for the NOP receptor (Table 4). Finally, it should be pointed out that the selectivity versus classical opioid receptors (μ, δ, and κ) of this novel scaffold for NOP receptor ligands is excellent given that no specific binding was observed at concentrations up to 400 nM.

Following chiral chromatographic resolution of (±)-31 and (±)-32, and single-crystal X-ray crystallography, the enantiomer with high binding affinity, (+)-31, was found to have *S*-configuration (see supporting information in ref 14). Conversely, the *R*-enantiomer, (-)-31, exhibited a markedly lower affinity for the NOP receptor (Table 4). Consistent data were generated with the (+)-32 enantiomer, which exhibited low NOP receptor binding affinity and has the *R*-configuration (see supporting information in ref 14). To assess the stereochemical stability of the chiral center, the compounds (+)-31 and (-)-32 were treated at 25 °C with sodium hydride and methyl iodide in dimethyl sulfoxide (Scheme 2). Chiral HPLC resolved the *N*-methylated products (-)-30 and (-)-33, respectively, in addition to the dimethylated compound (-)-27 and unchanged starting material (-)-32. Therefore, under basic alkylation conditions, racemization of the stereocenter does not occur and all products maintain the *S*-configuration (i.e., the products are (-)-30, (-)-27, and (-)-33). Thus, we have tentatively assigned the *S* configuration to all high affinity NOP enantiomers.

LC-MS/MS Tracer Evaluation in Rats. BP, SUV, and brain kinetics were evaluated with several analogues from the [4,5-dihydrothieno[2,3-*c*]pyran-7,4'-piperidine] scaffold. As it is shown in Table 5, the pyrazoles 8 and 19 differentially distributed in the CNS (indicated by the BP values) when administered in vivo. However, the reduced lipophilicity of 8 and 19, impaired brain penetration, as measured by SUV in vivo. Therefore, the correlation we have established between the calculated lipophilicities (clogD) and the measured log *D*, was overall predictive of good brain penetration for the majority of compounds. Previous studies have reported a similar relationship between CNS permeability and log *D*.²⁹ Thus, in an effort to maximize CNS penetration, the tracer SAR evolved to increase compound lipophilicity. Promising PET ligand candidates were identified from the tracer SAR using selection criteria of a BP greater than 2 following 3 μg/kg, iv at 40 min, and a %SUV greater than 100 at 10 min post dose. These two data points were found to select the best tracer ligands candidates for further evaluation as radiolabeled ligands. (+)-25, (-)-26, (-)-27, (-)-30, and (-)-33 exhibited specific binding in the hypothalamus (BP >1) and improved uptake, as measured by SUV. Interesting structural observations were noted when the thiophene ring was substituted by a chloro

Table 4. Opioid Receptor Binding Affinities and Functional Activities of the Novel NOP Antagonists 19–33



ligand	R ₁	R ₂	R ₃	NOP binding ^a K _i (nM)	NOP antagonist ^a K _b (nM)
(+)-19 ^c	F	CONMe ₂		0.248 (0.0262 n = 3)	0.225 (0.0764 n = 3)
(-)-20 ^{b,c}	Cl	CONMe ₂	Cl	0.169 (0.032 n = 2)	0.543 (0.033 n = 2)
(-)-21	Cl	CONMeH	Cl	0.124 (0.213 n = 2)	0.412 (0.217 n = 2)
(+)-22	Cl	CONH ₂	Cl	0.0373 (0.0277 n = 3)	0.167 (0.0524 n = 3)
(+)-23 ^{b,c}	Cl	CONMe ₂	F	0.0892 (0.0405 n = 3)	0.239 (0.0982 n = 3)
(-)-24	Cl	CONMeH	F	0.127 (0.0533 n = 3)	0.288 (0.112 n = 3)
(+)-25 ^b	F	CONMe ₂	Cl	0.134 (0.045 n = 2)	0.161 (0.055 n = 2)
(-)-26	F	CONMeH	Cl	0.0902 (0.0095 n = 3)	0.0992 (0.0278 n = 3)
(±)-27	F	CONMe ₂	F	0.396 (0.0799 n = 3)	0.698 (0.151 n = 3)
(-)-27 ^{b,c,d}	F	CONMe ₂	F	0.114 (0.0315 n = 3)	0.305 (0.0728 n = 3)
(-)-28	F	CONMe-cyPr	F	0.0672 (0.0179 n = 3)	0.085 (0.013 n = 3)
(-)-29	F	CONMe-cyPr	Cl	0.194 (0.0322 n = 2)	0.251 (0.156 n = 2)
(+)-30	F	CONMeH	F	5.32 (0.729 n = 2)	7.92 (3.00 n = 2)
(-)-30 ^e	F	CONMeH	F	0.174 (0.0106 n = 4)	0.189 (0.106 n = 2)
(-)-31	F	CONH ₂	F	5.61 (1.12 n = 7)	8.65 (3.00 n = 3)
(+)-31 ^f	F	CONH ₂	F	0.106 (0.022 n = 6)	0.173 (0.049 n = 3)
(+)-32 ^g	F	CONH-isoPr	F	4.54 (1.05 n = 2)	5.64 (1.05 n = 2)
(-)-32	F	CONH-isoPr	F	0.231 (0.05 n = 2)	0.288 (0.05 n = 2)
(-)-33	F	CONMe-isoPr	F	0.137 (0.028 n = 3)	0.141 (0.018 n = 3)

^aShown are geometric means (SEM, *n*) for K_i and K_b values. [³H]-Nociceptin was used as reference NOP radioligand in a binding assay using human recombinant NOP receptors expressed in CHO cells. Antagonist activity was determined in an assay of receptor-mediated G-protein activation using [³⁵S]-GTPγS and membranes expressing cloned human NOP receptors. ^bRadioligand binding with [³H]-diprenorphine, using membranes from CHO cells expressing human κ, μ, or δ opioid receptors gave K_i higher than 400 nM. ^cL-Tartaric acid salt. ^dRO tracer ligand. ^ePET tracer ligand. ^f¹⁴C absolute configuration determined by X-ray, compound (S)-9c in previous paper. ^gR absolute configuration determined by X-ray, compound (R)-9a in previous paper.¹⁴

Scheme 2. Chemical Correlation Reactions

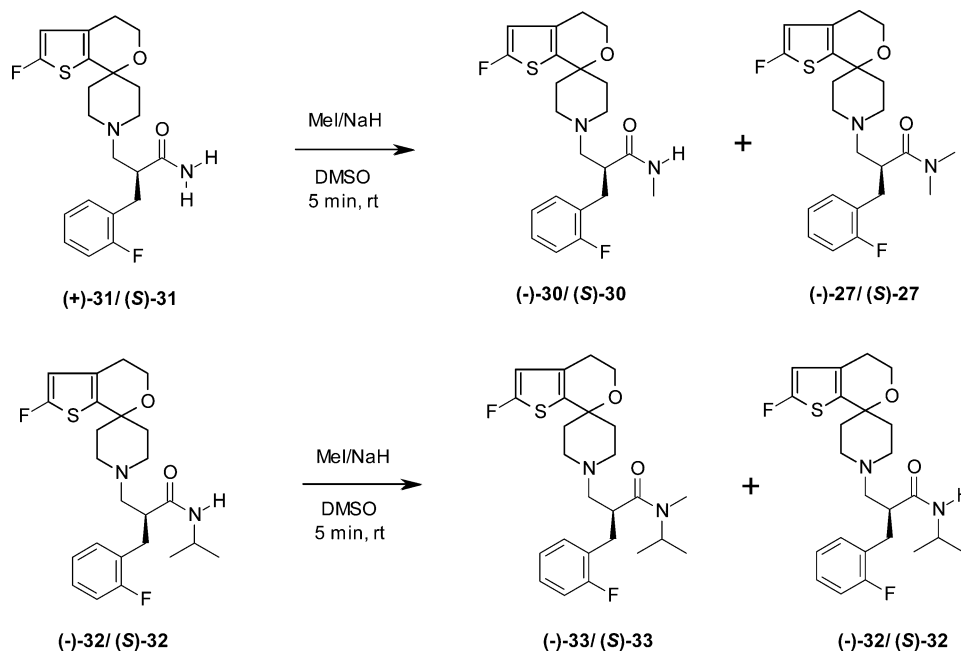
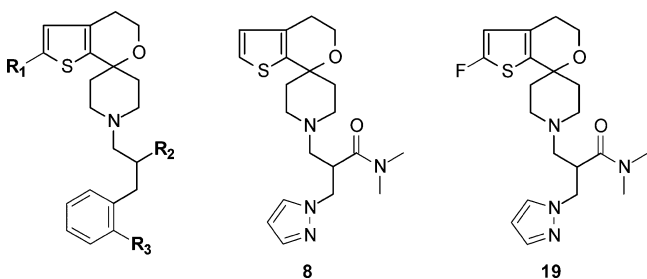


Table 5. Comparison of LC-MS/MS Evaluation of BP, Brain Uptake (SUV), and Lipophilicity (Calculated and Measured) of the Enantiomerically Pure NOP Antagonists 8, 19–30, and 33



ligand	R ₁	R ₂	R ₃	BP ^a	SUV ^b (%)	clogD ^c	log D ^d
(–)-8 ^e	H	CONMe ₂		0.8	15	1.48	2.03
(+)-19 ^e	F	CONMe ₂		3.5	65	1.69	2.84
(–)-20 ^e	Cl	CONMe ₂	Cl	2.0	75	3.89	4.61
(–)-21	Cl	CONMeH	Cl	1.9	87	3.64	3.77
(+)-22	Cl	CONH ₂	Cl	1.5	145	3.35	4.58
(+)-23 ^e	Cl	CONMe ₂	F	1.9	88	3.52	4.27
(–)-24	Cl	CONMeH	F	1.6	46	3.27	4.19
(+)-25	F	CONMe ₂	Cl	2.2	208	3.86	4.38
(–)-26	F	CONMeH	Cl	3.6	154	3.68	3.90
(–)-27 ^e	F	CONMe ₂	F	3.5	154	3.52	3.89
(–)-28	F	CONMe-cyPr	F	1.8	82	4.17	4.77
(–)-29	F	CONMe-cyPr	Cl	0.9	72	4.52	5.52
(–)-30	F	CONMeH	F	2.4	124	3.27	3.50
(–)-33	F	CONMe-isoPr	F	3.9	143	4.39	4.47

^a(BP) ratio of concentration of tracer in a hypothalamus versus striatum minus one. ^b(SUV) ratio of the concentration of the tracer in tissue to the injected tracer dose. ^cComputed with Pallas software. ^dlog D measured by the potentiometric method. ^eL-Tartaric acid salt.

atom at the 2 position (R₁ = Cl) as in (–)-20 to (–)-24, with the difference being halogen atom at the ortho position of the aryl group (R₃ = Cl or F) and the carboxamide. We found that while the signal-to-noise varied for the ligands, both BP and SUV were maintained. However, when the ortho substituent in the thiophene was a fluorine atom, as in (+)-25 to (–)-30 and (–)-33, the binding potentials were greater than 2 and SUV was greater than 100. Two notable exceptions were (–)-28 and (–)-29, which exhibited the highest measured log D but a low BP due to higher nonspecific binding. Our evaluation led us to conclude that the best potential tracers contain two fluorine atoms. Therefore, compound (–)-27 was selected as a preclinical tracer for further evaluation. Data from the rodent tracer evaluation for (–)-27 can be seen in Figure 1, where differential distribution was measured in hypothalamus, thalamus, and striatum. Higher specific binding can be seen in the receptor rich hypothalamus versus striatum producing a BP = 3.5. The brain concentration of (–)-27 diminishes after 60 min. The ratio of tissue concentrations of (–)-27 in hypothalamus and thalamus versus striatum demonstrated a consistent BP in receptor rich regions^{16,17} over the 60 min evaluation period (Figure 1B).

To complete our characterization, (–)-27 was evaluated in a blockade study with the known NOP receptor antagonist 3. Dose dependent blockade of tracer (–)-27 was demonstrated with 3, as shown in Figure 1C. Increasing doses of 3 were seen to dose dependently reduce brain concentrations of tracer compound (–)-27 in the hypothalamus, 1 h following oral

administration of 3, the time at which the tracer was administered. Little tracer blocking was observed in the striatum, low density NOP receptor region, supporting that the binding of (–)-27 is selective for the NOP receptor. Subsequently, receptor occupancy of compound 3 was determined using a 3 μg/kg, iv, dose of the unlabeled tracer compound (–)-27 following the oral administration of 3. Interestingly, compound 3 exhibited good in vivo potency, with a calculated ED₅₀ for NOP RO of 6.9 mg/kg (Figure 1D).

An optimized tracer suitable for PET ligand development needs high brain and plasma clearance for the desired kinetics amenable for carbon-11 imaging and should have limited CNS penetrant radiometabolites. In an effort to understand the mechanism of clearance associated with (–)-27, in vitro metabolic stability studies were conducted in rat, dog, monkey, and human microsomes. Moreover, metabolite profiling was conducted using cryopreserved hepatocytes isolated from the same species because oxidative metabolism was thought to be a predominant clearance pathway for the molecule. The LC-MS/MS profiling of these samples showed oxidative N-demethylation to be a primary pathway of clearance for (–)-27 (data not shown). To reduce the potential formation of radiometabolites resulting from N-demethylation, we evaluated the monomethylated high affinity ligands, (–)-26 and (–)-30 and the isopropyl derivative (–)-33. All three compounds possess a potential site for radiolabeling as well as excellent binding potential and brain penetration in vivo (Table 5). Of the three compounds, [¹¹C]-(S)-30 was identified as an efficient PET radioligand due to its good brain entry, most favorable kinetics, and large receptor-specific signal in rat and monkey brain in vivo as previously reported.^{14,15}

SUMMARY

We have identified the 3-(2'-fluoro-4',5'-dihydrospiro[piperidine-4,7'-thieno[2,3-c]pyran]-1-yl)-2(2-halobenzyl)-N-alkylpropanamides as a chemotype with high affinity and selectivity for the NOP receptor. In rats, we optimized the SAR to produce compounds with subnanomolar binding affinities, high selectivity, low nonspecific binding, and high brain uptake. Consequently, we have identified (–)-27 as a novel unlabeled receptor occupancy tracer which allows preclinical high throughput determination of rat brain NOP occupancy and [¹¹C]-(S)-30 as a PET radiotracer.

EXPERIMENTAL SECTION

Materials and Methods. All reagents used were obtained from commercial sources (Sigma-Aldrich, unless otherwise stated). All solvents were of an analytical grade. The NOP agonist ligands Ro 64-6198,²³ W-212393,²⁵ NNC 63-0532,²⁶ and the antagonist ligands J-113397,²⁴ SB-612111,²⁷ and (–)-4²⁸ were synthesized as reported. [³⁵S]-GTPγS was obtained commercially. Preparation of racemic and enantiomerically pure 26, 30, 31, 32, and 33 was according to previously reported methods.¹⁴

Isolation of compounds by column chromatography was performed on silica gel columns (SP1a HPFC system, Biotage Inc., Charlottesville, VA).

LC-MS was performed with an 1100 series LC-MSD single quadrupole instrument (Agilent; Santa Clara, CA) with an ESI interface.

The purity of synthesized ligands was found to be ≥95% by the following described LC-MS methods 1–5 as specified in each case.

Method 1: Used a heated (50 °C) XBridge C18 column (3.5 μm; 2.1 mm × 50 mm; Waters, Milford, MA) eluted at 1 mL/min with a gradient of A (10 mM aq NH₄HCO₃; pH 9) and B (MeCN), with B increased linearly from 10% to 100% (v/v) over 3.5 min. Ions between m/z 100–750 were captured after electrospray ionization of the eluted test sample.

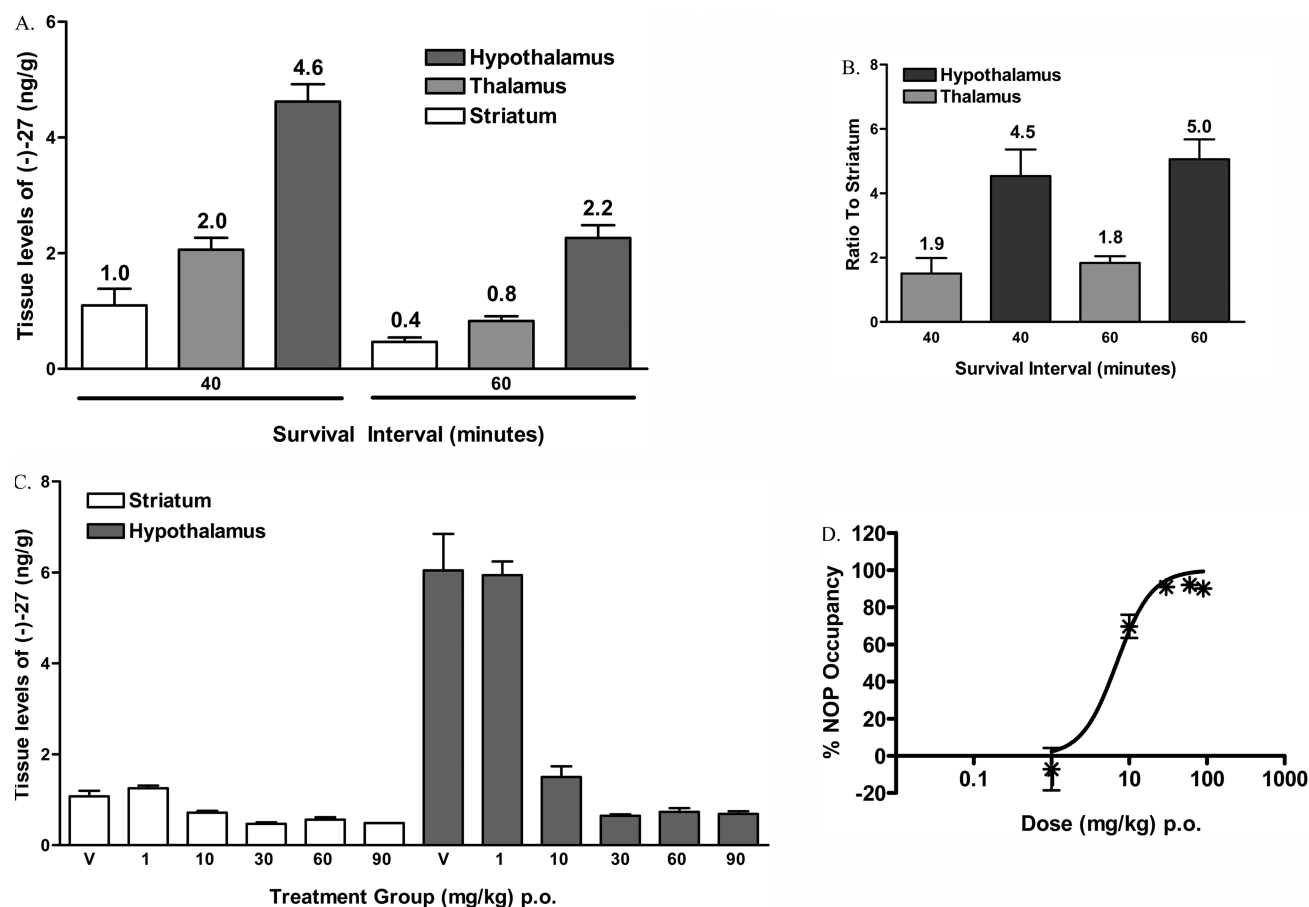


Figure 1. (A) Brain concentrations of (–)-27 40 and 60 min post iv injection of the compound at a dose of 3 $\mu\text{g}/\text{kg}$ in male HSD rats. (B) Ratio of hypothalamic and thalamic (–)-27 tracer levels to those measured in striatum in male HSD rats. (C) Brain concentrations of unlabeled tracer compound (–)-27 in total (hypothalamus) and nonspecific (striatum) binding tissues following oral administration of vehicle (V) or 3 (SB-61211). Tracer dose of (–)-27 was 3 $\mu\text{g}/\text{kg}$ with a 40 min survival interval. (D) Orally administered 3 (SB-61211) dose dependently occupies NOP receptors in rat hypothalamus, as assessed with unlabeled tracer (–)-27. NOP occupancy was calculated using the ratio method for the data set in (C).

Method 2: Used a heated (45 °C) CAPCELL PAK C18 MG column (3.0 μm ; 4.6 mm \times 35 mm), eluted at 1.2 mL/min with a gradient of H₂O (0.05% trifluoroacetic acid (TFA) (A)/MeCN (0.05% TFA) (B), with B increased linearly from 10% to 95% (v/v) over 2.4 min. Detection: UV (214.4 nm). Ions between m/z 80–800 were captured after electrospray ionization of the eluted test sample.

Method 3: Used a heated (50 °C) Gemini C18 column (3.0 μm ; 2.0 mm \times 50 mm), eluted at 1.0 mL/min, with a gradient of H₂O (0.05%TFA) (A)/MeCN (0.05%TFA) (B), with B increased linearly from 5% to 100% over 7 min. Detection: UV (214.4 nm). Ions between m/z 70–800 were captured after electrospray ionization of the eluted test sample.

Method 4: Used a heated (50 °C) Gemini C18 (3.0 μm ; 2.0 mm \times 50 mm), eluted at 1.0 mL/min with a gradient of H₂O (0.1% formic acid) (A)/MeCN (0.1% formic acid) (B), with B increased from 5% to 100% over 7 min. Detection: UV (214.4 nm). Ions between m/z 70–800 were captured after electrospray ionization of the eluted test sample.

Method 5: Used a heated (50 °C) SepaxBR-C18 column (3.0 μm ; 2.1 mm \times 50 mm), eluted at 1.0 mL/min with a gradient of H₂O (10 mmol NH₄HCO₃) (A)/MeCN (B), with B increased from 10% to 100% over 7 min. Detection: UV (214.4 nm). Ions between m/z 70–800 were captured after electrospray ionization of the eluted test sample.

Chiral HPLC method 1: HPLC, Chiralpak AD 20 mm \times 250 mm, 0.2% dimethylethylamine (DMEA) in hexane/EtOH (90:10 v/v). Flow rate of 12 mL/min. λ = 254 nm.

Chiral HPLC method 2: HPLC, Chiralpak AD-H 4.6 mm \times 250 mm, 0.1% diethylamine (DEA) in hexane/EtOH (90:10 v/v). Flow rate of 15 mL/min. λ = 214 and 254 nm.

High-resolution mass spectrometry (HRMS) was performed on an TOF/Q-TOF instrument (Agilent). Data were acquired in dual ESI mode (+ and –) in the range of 95–1700 amu. The sample (~0.1 mg/mL in MeCN-H₂O, 1:1 v/v; 2 μL) was injected in loop mode onto a Zorbax SB-C8 column (3.5 μm ; 3.0 mm \times 150 mm; Agilent) eluted at 0.5 mL/min with a mixture of 0.1% formic acid in H₂O (A) and 0.1% formic acid in MeCN (B) with B increasing from 5 to 100% over 15 min and then held at 100% for 8 min. Eluate was monitored with a diode array detector operating in the range 190–700 nm.

¹H NMR (300 MHz) spectra were acquired at 20 °C on a System 300 instrument (Varian; Palo Alto, CA). Abbreviations s, d, dd, ddd, m, and br denote singlet, doublet, double doublet, double double doublet, multiplet, and broad, respectively.

Optical rotations were measured with a 341 polarimeter (Perkin-Elmer) at 20 °C and at 589 nm (sodium lamp).

Statistics. Values are given as means \pm the standard deviation of the mean unless otherwise stated.

Animals. Male Sprague–Dawley rats (Harlan Sprague–Dawley, Indianapolis, IN), weighing between 230 and 280 g, were used for in vivo experiments. All rats were housed in rooms using a 12 h light/dark cycle and had ad lib access to normal rat chow and H₂O until the beginning of the 3 h experimental protocol. All experiments with rats were performed in accord with the National Research Council Guide under protocols approved by the Animal Care and Use Committee of Eli Lilly and Company.

Chemistry. 2-Chlorospiro[4,5-dihydrothieno[2,3-c]pyran-7,4'-piperidine] (**6c**). Step 1: *N*-Chlorosuccinimide (2.63 g, 19.39 mmol) was added to a solution of *tert*-butyl spiro[4,5-dihydrothieno[2,3-c]pyran-7,4'-piperidine]-1'-carboxylate¹⁴ (5 g, 16.16 mmol) in acetonitrile (6 mL). The resulting mixture was heated to 70 °C overnight. The reaction was allowed to reach room temperature (rt), and the solvent was evaporated. The oily residue was dissolved in methyl *tert*-butyl ether (MTBE) (20 mL). Hexane (200 mL) was added, and the resulting mixture was stirred at rt for 1 h. The solid was filtered off, and the filtrate was concentrated to give *tert*-butyl 2-chlorospiro[4,5-dihydrothieno[2,3-c]pyran-7,4'-piperidine]-1'-carboxylate as a yellow solid (5.5 g, 99%). LC-MS (ESI): *m/z* 287 (MH)⁺, 243, *t_R* = 2.84 min, purity 100%, method 1. ¹H NMR (300 MHz, CDCl₃): 6.59 (s, 1H), 3.99–3.89 (m, 4H), 3.11 (td, *J* = 13.0, 2.5 Hz, 2H), 2.60 (t, *J* = 5.5 Hz, 2H), 1.97 (dd, *J* = 1.9, 14.3 Hz, 2H), 1.74–1.60 (m, 2H), 1.48 (s, 9H). HRMS (ESI): calcd for C₁₆H₂₂ClNO₃S, 343.1008; found, 343.1009. Step 2: HCl (4M) solution in dioxane (2.5 mL, 10 mmol) was added to a solution of the compound obtained in step 1 (380 mg, 1.1 mmol) in dioxane (2.5 mL), and the resulting mixture was stirred at rt. When the reaction was completed, the solvent was evaporated under vacuum and the residue partitioned in CH₂Cl₂ and NaOH (1N). The organic layer was separated, dried over MgSO₄, and evaporated to yield **6c** (264 mg, 98%) as a yellow solid. LC-MS (ESI): *m/z* 243 (MH)⁺, *t_R* = 2.65 min, purity 100%, method 1. ¹H NMR (300 MHz, CDCl₃): 6.57 (s, 1H), 3.90 (t, *J* = 5.5 Hz, 3H), 3.08–2.90 (m, 5H), 2.59 (t, *J* = 5.4 Hz, 3H), 2.00 (d, *J* = 13.3 Hz, 3H), 1.80–1.68 (m, 3H). HRMS (ESI): calcd for C₁₁H₁₄ClNOS, 243.049; found, 243.0485.

General Michael Addition Procedure. Triethylamine (TEA) (2.48 g, 19.34 mmol) and the corresponding alkyl acrylate were added to a solution of the piperidine intermediate (**6a–6c**) (9.67 mmol) dissolved in MeOH (50 mL). The crude mixture was refluxed overnight. The reaction mixture was cooled to rt and the solvent removed under vacuum. The resulting crude product was purified by flash chromatography.

***tert*-Butyl 3-(4',5'-Dihydro-1H-spiro[piperidine-4,7'-thieno[2,3-c]pyran]-1-yl) Propanoate (7a).** The title compound was obtained from **6a** (870 mg, 4.16 mmol) and *tert*-butyl acrylate (984 mg, 7.68 mmol) according to the general Michael addition procedure. The crude product was purified by a plug of silica gel (CH₂Cl₂) to furnish **7a** (1.3 g, 93%) as a colorless solid. LC-MS (ESI): *m/z* 338 (M + H)⁺. ¹H NMR (300 MHz, CDCl₃) δ 7.17 (d, *J* = 5.1 Hz, 1H), 6.75 (d, *J* = 5.1 Hz, 1H), 3.91 (t, *J* = 5.7 Hz, 2H), 2.74–2.66 (m, 6H), 2.48–2.39 (m, 4H), 2.04–1.93 (m, 4H), 1.45 (s, 9H).

***tert*-Butyl 3-(2'-Chloro-4',5'-dihydro-1H-spiro[piperidine-4,7'-thieno[2,3-c]pyran]-1-yl)propanoate (7c).** The title compound was obtained from **6c** (2.35 g, 9.67 mmol) and *tert*-butyl acrylate (2.44 g, 24.18 mmol) according to the general Michael addition procedure. The crude product was purified by flash chromatography (CH₂Cl₂/MeOH = 40:1) to furnish **7c** (3.2 g, 89%) as a light-yellow oil. LC-MS (ESI): *m/z* 372 (M + H)⁺.

3-(2'-Fluoro-4',5'-dihydro-1H-spiro[piperidine-4,7'-thieno[2,3-c]pyran]-1-yl)-2-(1H-pyrazol-1-ylmethyl)propionic Acid. Step 1: Ethyl 2-((1H)-pyrazol-1-ylmethyl)acrylate²⁸ (150 mg, 0.83 mmol) was added to a solution of **6b**¹⁴ (173 mg, 0.76 mmol) according to the general Michael addition procedure. The crude product was purified by preparative thin-layer chromatography (TLC) (petroleum ether/ethyl acetate = 1:1) to yield ethyl 3-(2'-fluoro-4',5'-dihydro-1H-spiro[piperidine-4,7'-thieno[2,3-c]pyran]-1-yl)-2-(1H-pyrazol-1-ylmethyl)propanoate (57 mg, 18%) as a yellow oil. LC-MS (ESI): *m/z* 408 (M + H)⁺. ¹H NMR (300 MHz, CDCl₃) δ 7.50 (d, *J* = 1.5 Hz, 1H), 7.38 (d, *J* = 1.8 Hz, 1H), 6.20 (t, *J* = 1.8 Hz, 1H), 6.11 (d, *J* = 1.5 Hz, 1H), 4.40 (d, *J* = 7.2 Hz, 2H), 4.05–4.19 (m, 2H), 3.89 (t, *J* = 5.7 Hz, 2H), 3.24–3.35 (m, 1H), 2.35–2.76 (m, 7H), 1.94–2.02 (m, 2H), 1.62–1.85 (m, 3H), 1.20 (t, *J* = 7.2 Hz, 3H). Step 2: LiOH monohydrate (18 mg, 0.43 mmol) in THF (1 mL) and H₂O (2 mL) was added to a solution of the compound obtained in step 1 (55 mg, 0.14 mmol) in THF (1 mL). The reaction mixture was stirred at rt for 16 h, acidified to pH 2 with HCl solution (1N), and extracted with ethyl acetate. The combined organic extracts were dried over Na₂SO₄, filtered, and concentrated under vacuum

to afford the title compound (41 mg, 80%) as a yellow oil. LC-MS (ESI): *m/z* 380 (M + H)⁺. ¹H NMR (300 MHz, CDCl₃) δ 7.49–7.59 (m, 2H), 6.55 (br, 1H), 6.25 (s, 1H), 6.14 (s, 1H), 4.61–4.65 (m, 1H), 4.44–4.50 (m, 1H), 3.88 (t, *J* = 5.4 Hz, 2H), 3.43–3.47 (m, 1H), 3.22–3.33 (m, 3H), 3.06–3.11 (m, 1H), 2.82–3.00 (m, 2H), 2.55 (t, *J* = 4.8 Hz, 2H), 2.00–2.60 (m, 4H).

2-(Methylenepyrazole)-3-[spiro(benzothiophene-1(3H),4'-piperidine)propionic Acid. Step 1: Ethyl 2-((1H)-pyrazol-1-ylmethyl)acrylate²⁸ (150 mg, 0.86 mmol) was added to a solution of **6a**¹⁴ (160 mg, 0.78 mmol) according to the general Michael addition procedure. The crude product was purified by preparative TLC (petroleum ether/ethyl acetate = 2:3) to yield ethyl 2-(methylenepyrazole)-3-[spiro(benzothiophene-1(3H),4'-piperidin)propanoate (200 mg, 67%) as a yellow oil. LC-MS (ESI): *m/z* 390 (MH)⁺. ¹H NMR (300 MHz, CDCl₃): 7.50 (dd, *J* = 0.5, 1.8 Hz, 1H), 7.39 (dd, *J* = 0.5, 2.4 Hz, 1H), 7.13 (d, *J* = 5.1 Hz, 1H), 6.76 (d, *J* = 5.1 Hz, 1H), 6.20 (t, *J* = 2.1 Hz, 1H), 4.42–4.39 (m, 2H), 4.15–4.08 (m, 2H), 3.90 (t, *J* = 5.5 Hz, 2H), 3.27 (q, 1H), 2.72–2.52 (m, 8H), 2.03–1.90 (m, 4H), 1.19 (t, *J* = 7.1 Hz, 3H). Step 2: The compound obtained in step 1 was hydrolyzed with LiOH according to the same procedure used for the preparation of compound 3-(2'-fluoro-4',5'-dihydro-1H-spiro[piperidine-4,7'-thieno[2,3-c]pyran]-1-yl)-2-(1H-pyrazol-1-ylmethyl)propionic acid. The title compound (85 mg, 75%) was obtained as a colorless oil. LC-MS (ESI): *m/z* 362 (MH)⁺. ¹H NMR (300 MHz, CDCl₃): 7.49 (d, *J* = 2.0 Hz, 1H), 7.42 (d, *J* = 1.6 Hz, 1H), 7.11 (d, *J* = 5.0 Hz, 1H), 6.73 (d, *J* = 5.0 Hz, 1H), 6.16 (t, *J* = 2.1 Hz, 1H), 4.56–4.34 (m, 2H), 3.84 (t, *J* = 5.4 Hz, 2H), 3.11–2.90 (m, 4H), 2.72–2.49 (m, 5H), 2.14–1.95 (m, 4H).

General Condensation Procedure. A solution of LiN(TMS)₂ (1M) in dry THF (7.48 mL, 7.48 mmol) was added dropwise to a stirred solution of **7a–7c** (3.74 mmol) in dry THF (12 mL) at –78 °C. After 1 h of stirring, 1,3-dimethyl-tetrahydropyrimidin-2(1H)-one (0.45 mL, 3.74 mmol) was added at –78 °C and the resulting mixture stirred for 30 min. Then the corresponding benzyl bromide (4.13 mmol) in dry THF (10 mL) was added. Stirring was continued for 1 h, and the temperature was allowed to rise to 0 °C, where it was kept for 1 h. Saturated aqueous NH₄Cl solution was added. The mixture was extracted twice with ethyl acetate and the combined organic extracts dried over Na₂SO₄ and evaporated under vacuum. The resulting crude product was purified by chromatography.

Amide Formation General Procedure. TFA (2 mL) was added to a stirred solution of the ester (0.37 mmol) in dichloromethane (2 mL), and stirred at rt for 18 h. The reaction mixture was evaporated to dryness to afford the trifluoroacetate salt of the corresponding propionic acid which was used without further purification. 1-Hydroxybenzotriazole (HOBt) (61 mg, 0.45 mmol) and 1-ethyl-3(dimethylaminopropyl)-carbodiimide (EDCI) (86 mg, 0.45 mmol) in dry dichloromethane (20 mL) were added to a stirred solution of the trifluoroacetate salt (0.37 mmol) and the corresponding amine hydrochloride (0.37 mmol). Then di-isopropylethylamine (DIPEA) (173.8 μL, 1.0 mmol) was added, and the mixture was stirred at rt for 18 h. The reaction mixture was washed with HCl (1N) and brine, dried over Na₂SO₄, and concentrated under vacuum. The resulting crude product was purified by chromatography.

***L*-Tartaric Salt Formation General Procedure.** *L*-Tartaric acid (1 equiv) was added to a stirred solution of the free base (1 equiv) in methanol. Evaporation of the solvent followed by trituration with diethyl ether gave rise to the corresponding salt.

2-(Pyrazol-1-ylmethyl)-3-spiro[4,5-dihydrothieno[2,3-c]pyran-7,4'-piperidine]-1'-yl-*N,N*-dimethylpropanamide ((±)-8). The racemic title compound was prepared from 2-(methylenepyrazole)-3-[spiro(benzothiophene-1(3H),4'-piperidine)propionic acid (560 mg, 1.56 mmol) and dimethylamine hydrochloride (127 mg, 1.56 mmol) according to the general amide formation procedure. The crude product was purified by preparative HPLC (hexane/ethyl acetate = 8:1) to afford **8** (385 mg, 64%) as a yellow oil. LC-MS (ESI): *m/z* 389 (MH)⁺, *t_R* = 1.98 min, purity 96%, method 1. ¹H NMR (300 MHz, CDCl₃): 7.47 (s, 1H), 7.34 (s, 1H), 7.10 (dd, *J* = 1.3, 4.9 Hz, 1H), 6.74–6.72 (m, 1H), 6.17–6.14 (m, 1H), 4.44–4.30 (m, 2H), 3.87 (t, *J* = 5.4 Hz, 2H), 3.69–3.60 (m, 1H), 2.84 (d, *J* = 1.3 Hz, 3H), 2.79

(d, $J = 1.3$ Hz, 3H), 2.74–2.64 (m, 5H), 2.56–2.46 (m, 3H), 2.01–1.85 (m, 4H).

Resolution of (\pm)-8 by chiral HPLC method 1 (at 150 mL/min flow rate) gave (–)-8 ($t_R = 5.39$ min) and (+)-8 ($t_R = 6.87$ min). (–)-8: LC-MS (ESI): m/z 389 ($M + H$)⁺, $t_R = 1.75$ min, purity 100%, method 1. The L-tartaric salt was prepared according to the general L-tartaric salt formation procedure. $[\alpha]_D -16.2^\circ$ (c 0.5, MeOH). HRMS (ESI): calcd for C₂₀H₂₈N₄O₂S, 388.1933, found 388.1944. (+)-8: LC-MS (ESI) m/z 389 ($M + H$)⁺, $t_R = 1.75$ min, purity 100%, method 1. The L-tartaric salt was prepared. $[\alpha]_D +16.6^\circ$ (c 0.5, MeOH). HRMS (ESI): calcd for C₂₀H₂₈N₄O₂S, 388.1933; found, 388.1934.

3-(2'-Fluoro-4',5'-dihydro-1H-spiro[piperidine-4,7'-thieno[2,3-c]pyran]-1-yl) 2-(1H-pyrazol-1-ylmethyl)-N,N-dimethylpropanamide ((±)-19). The racemic title compound was prepared from 3-(2'-fluoro-4',5'-dihydro-1H-spiro[piperidine-4,7'-thieno[2,3-c]pyran]-1-yl) 2-(1H-pyrazol-1-ylmethyl)propionic acid (41 mg, 0.11 mmol) and dimethylamine hydrochloride (8.91 mg, 0.11 mmol) according to the general amide formation procedure. The crude product was purified by preparative HPLC (hexane/ethyl acetate = 8:1) to afford (±)-19 (16 mg, 36%) as a colorless oil. LC-MS (ESI): m/z 407 ($M + H$)⁺, $t_R = 3.05$ min, purity 93.7%, method 1. ¹H NMR (300 MHz, CDCl₃) δ 7.49 (d, $J = 1.8$ Hz, 1H), 7.35 (d, $J = 2.7$ Hz, 1H), 6.17 (t, $J = 2.1$ Hz, 1H), 6.11 (d, $J = 1.8$ Hz, 1H), 4.28–4.44 (m, 2H), 3.89 (t, $J = 5.1$ Hz, 2H), 3.60–3.70 (m, 1H), 2.05 (s, 3H), 2.79 (s, 3H), 2.62–2.78 (m, 3H), 2.32–2.56 (m, 5H), 1.93–2.01 (m, 2H), 1.70–1.83 (m, 2H).

Resolution of (±)-19 by chiral HPLC method 1 gave (+)-19 ($t_R = 9.82$ min) and (–)-19 ($t_R = 12.27$ min). (+)-19: LC-MS (ESI) m/z 407 ($M + H$)⁺, $t_R = 1.88$ min, purity 100%, method 1. The L-tartaric salt was prepared. $[\alpha]_D +15.3^\circ$ (c 0.5, MeOH). HRMS (ESI): calcd for C₂₀H₂₇FN₄O₂S, 406.1839, found 406.1848.

2-Chlorophenylmethyl-3-(2-chlorospiro[4,5-dihydrothieno[2,3-c]pyran-7,4'-piperidine]-1'-yl)-N,N-dimethylpropanamide ((±)-20). The racemic title compound was prepared from *tert*-butyl 2-[(2-chlorophenyl)methyl]-3-(2-chlorospiro[4,5-dihydrothieno[2,3-c]pyran-7,4'-piperidine]-1'-yl)propanoate (241 mg, 0.51 mmol) and dimethylamine hydrochloride (42 mg, 0.51 mmol) according to the general amide formation procedure. The crude product was purified by preparative HPLC (hexane/ethyl acetate = 8:1) to afford (±)-20 (50 mg, 22%) as a colorless oil.

Resolution of (±)-20 by chiral HPLC method 1 gave (–)-20 ($t_R = 6.17$ min) and (+)-20 ($t_R = 9.01$ min). (–)-20: The L-tartaric salt was prepared. LC-MS (ESI): m/z 467 ($M + H$)⁺, $t_R = 4.79$ min, purity 100%, method 1. ¹H NMR (300 MHz, CDCl₃) δ 7.34–7.31 (m, 1H), 7.21–7.13 (m, 3H), 6.57 (s, 1H), 3.87 (t, $J = 5.7$ Hz, 2H), 3.48–3.36 (m, 1H), 3.15–3.06 (m, 1H), 2.93–2.78 (m, 5H), 2.75–2.62 (m, 5H), 2.59–2.37 (m, 5H), 1.95 (d, $J = 13.8$ Hz, 2H), 1.82–1.78 (m, 2H). $[\alpha]_D -30.4^\circ$ (c 0.52, MeOH).

2-Chlorophenylmethyl-3-(2-chlorospiro[4,5-dihydrothieno[2,3-c]pyran-7,4'-piperidine]-1'-yl)-N-methylpropanamide ((±)-21). The racemic title compound was prepared from *tert*-butyl 2-[(2-chlorophenyl)methyl]-3-(2-chlorospiro[4,5-dihydrothieno[2,3-c]pyran-7,4'-piperidine]-1'-yl)propanoate (330 mg, 0.66 mmol) and methyl amine hydrochloride (45 mg, 0.66 mmol) according to the general amide formation procedure. The crude product was purified by preparative TLC (CH₂Cl₂/MeOH = 25:1) to afford (±)-21 (220 mg, 73%) as a white solid.

Resolution of (±)-21 by chiral HPLC method 1 (at 250 mL/min flow rate) gave (–)-21 ($t_R = 6.08$ min) and (+)-21 ($t_R = 8.08$ min). (–)-21: LC-MS (ESI): m/z 453 ($M + H$)⁺, $t_R = 4.31$ min, purity 100%, method 1. ¹H NMR (300 MHz, CDCl₃) δ 7.34–7.25 (m, 2H), 7.19–7.14 (m, 2H), 6.57 (s, 1H), 3.87 (t, 2H, $J = 5.4$ Hz), 3.27–3.21 (m, 1H), 2.86–2.65 (m, 5H), 2.76 (d, 3H, $J = 4.8$ Hz), 2.59 (t, 2H, $J = 5.4$ Hz), 2.53–2.39 (m, 2H), 2.29–2.20 (m, 1H), 2.00–1.96 (m, 2H), 1.83–1.75 (m, 2H). $[\alpha]_D -24.4^\circ$ (c 5.0, MeOH). HRMS (ESI): calcd for C₂₂H₂₆Cl₂N₂O₂S, 452.1092; found, 452.1096.

2-Chlorophenylmethyl-3-(2-chlorospiro[4,5-dihydrothieno[2,3-c]pyran-7,4'-piperidine]-1'-yl)propanamide ((±)-22). The racemic title compound was prepared from *tert*-butyl 2-[(2-chlorophenyl)methyl]-3-(2-chlorospiro[4,5-dihydrothieno[2,3-c]pyran-7,4'-piperidine]-1'-yl)-

propanoate (119 mg, 0.24 mmol) and ammonium chloride (12.8 mg, 0.24 mmol) according to the general amide formation procedure. The crude product was purified by preparative TLC (CH₂Cl₂/MeOH = 20:1) to afford (±)-22 (75 mg, 71%) as a white solid.

Resolution of (±)-22 by chiral HPLC method 2 gave (–)-22 ($t_R = 10.17$ min) and (+)-22 ($t_R = 12.50$ min). (+)-22: LC-MS (ESI) 439 ($M + H$)⁺, $t_R = 4.17$ min, purity 95%, method 1. ¹H NMR (300 MHz, CDCl₃) δ 7.66 (brs, 1H), 7.36–7.27 (m, 2H), 7.22–7.14 (m, 2H), 7.58 (s, 1H), 5.41 (brs, 1H), 3.87 (t, 2H, $J = 5.4$ Hz), 3.34–3.28 (q, 1H, $J = 5.1$ Hz), 2.89–2.64 (m, 5H), 2.59 (t, 2H, $J = 5.4$ Hz), 2.52–2.36 (m, 2H), 2.24–2.15 (m, 1H), 2.05–1.70 (m, 4H). $[\alpha]_D +6.4^\circ$ (c 1.0, EtOH). HRMS (ESI): calcd for C₂₁H₂₅Cl₂N₂O₂S + H⁺, 439.1008; found, 439.1021.

2-Fluorophenylmethyl-3-(2-chlorospiro[4,5-dihydrothieno[2,3-c]pyran-7,4'-piperidine]-1'-yl)-N,N-dimethylpropanamide ((±)-23). The racemic title compound was prepared from *tert*-butyl 2-[(2-fluorophenyl)methyl]-3-(2-chlorospiro[4,5-dihydrothieno[2,3-c]pyran-7,4'-piperidine]-1'-yl)propanoate (136 mg, 0.28 mmol) and dimethylamine hydrochloride (23 mg, 0.28 mmol) according to the general amide formation procedure. The crude product was purified by preparative TLC (CH₂Cl₂/MeOH = 20:1) to afford (±)-23 (60 mg, 47%) as a light-yellow oil.

Resolution of (±)-23 by chiral HPLC method 1 gave (+)-23 ($t_R = 6.44$ min) and (–)-23 ($t_R = 8.78$ min). (+)-23: LC-MS (ESI) 451 ($M + H$)⁺, $t_R = 4.45$ min, purity 97.5%, method 1. ¹H NMR (300 MHz, CDCl₃) δ 7.13–7.22 (m, 2H), 6.95–7.11 (m, 2H), 6.56 (s, 1H), 3.86 (t, $J = 5.1$ Hz, 2H), 3.25–3.35 (m, 1H), 2.75–3.02 (m, 9H), 2.30–2.70 (m, 7H), 1.90–2.00 (m, 2H), 1.70–1.85 (m, 2H). The L-tartaric salt was prepared. $[\alpha]_D +6.4^\circ$ (c 1.0, EtOH). HRMS (ESI): calcd for C₂₃H₂₉ClFN₂O₂S + H⁺, 451.1617; found, 451.1624.

2-Fluorophenylmethyl-3-(2-chlorospiro[4,5-dihydrothieno[2,3-c]pyran-7,4'-piperidine]-1'-yl)-N-methylpropanamide ((±)-24). The racemic title compound was prepared from *tert*-butyl 2-[(2-fluorophenyl)methyl]-3-(2-chlorospiro[4,5-dihydrothieno[2,3-c]pyran-7,4'-piperidine]-1'-yl)propanoate (742 mg, 1.54 mmol) and methyl amine hydrochloride (104 mg, 1.54 mmol) according to the general amide formation procedure. The crude product was purified by preparative TLC (CH₂Cl₂/MeOH = 25:1) to afford (±)-24 (392 mg, 58%) as a white solid.

Resolution of (±)-24 by chiral HPLC method 2 gave (–)-24 ($t_R = 6.43$ min) and (+)-24 ($t_R = 8.50$ min). (–)-24: LC-MS (ESI) 437 ($M + H$)⁺, $t_R = 4.74$ min, purity 100%, method 3. ¹H NMR (300 MHz, CDCl₃) δ 7.46 (br, 1H), 7.15–7.25 (m, 2H), 6.96–7.07 (m, 2H), 6.57 (s, 1H), 3.85 (t, $J = 5.4$ Hz, 2H), 3.15–3.21 (m, 1H), 2.52–2.79 (m, 10H), 2.37–2.52 (m, 2H), 2.22 (td, $J = 2.4$ Hz, 1H), 1.95–2. $[\alpha]_D -7.0^\circ$ (c 1.0, EtOH). HRMS (ESI): calcd for C₂₂H₂₆ClFN₂O₂S, 436.1387; found, 436.1388.

3-(2'-Fluoro-4',5'-dihydro-1H-spiro[piperidine-4,7'-thieno[2,3-c]pyran]-1-yl) 2-(2-Chlorobenzyl)-N,N-dimethylpropanamide ((±)-25). The racemic title compound was prepared from *tert*-butyl 2-[(2-chlorophenyl)methyl]-3-(2-fluorospiro[4,5-dihydrothieno[2,3-c]pyran-7,4'-piperidine]-1'-yl)propanoate¹⁴ (188 mg, 0.39 mmol) and dimethylamine hydrochloride (32 mg, 0.39 mmol) according to the general amide formation procedure. The crude product was purified by column chromatography in silica gel (CH₂Cl₂/MeOH = 30:1) to afford (±)-25 (120 mg, 68%) as a pale yellow solid.

Resolution of (±)-25 by chiral HPLC method 1 gave (+)-25 ($t_R = 5.67$ min) and (–)-25 ($t_R = 7.85$ min). (+)-25: LC-MS (ESI) 451 ($M + H$)⁺, $t_R = 4.45$ min, purity 97.8%, method 1. ¹H NMR (300 MHz, CDCl₃) δ 7.31–7.34 (m, 1H), 7.13–7.21 (m, 3H), 6.11 (d, $J = 1.5$ Hz, 1H), 3.89 (t, $J = 5.4$ Hz, 2H), 3.35–3.45 (m, 1H), 3.10–3.16 (m, 1H), 2.77–2.87 (m, 5H), 2.81–2.75 (m, 5H), 2.37–2.55 (m, 3H), 2.32–2.45 (m, 2H), 1.93–1.98 (m, 2H), 1.67–1.81 (m, 2H). $[\alpha]_D +42.6^\circ$ (c 1.0, EtOH). HRMS (ESI): calcd for C₂₃H₂₉ClFN₂O₂S + H⁺, 451.1617; found, 451.1624.

3-(2'-Fluoro-4',5'-dihydro-1H-spiro[piperidine-4,7'-thieno[2,3-c]pyran]-1-yl) 2-(2-Fluorobenzyl)-N,N-dimethylpropanamide ((±)-27). The racemic title compound was prepared from *tert*-butyl 2-[(2-fluorophenyl)methyl]-3-(2-fluorospiro[4,5-dihydrothieno[2,3-c]pyran-7,4'-piperidine]-1'-yl)propanoate¹⁴ (1.46 g, 3.15 mmol) and

dimethylamine hydrochloride (257 mg, 3.15 mmol) according to the general amide formation procedure. The crude product was purified by preparative TLC ($\text{CH}_2\text{Cl}_2/\text{MeOH} = 20:1$) to afford (\pm)-27 (550 mg, 40%) as a light-yellow oil. LC-MS (ESI) 435 ($\text{M} + \text{H}$)⁺, $t_{\text{R}} = 4.15$ min, purity 98.0%, method 1. ¹H NMR (300 MHz, CDCl_3) δ 7.14–7.19 (m, 2H), 6.96–7.04 (m, 2H), 6.10 (d, $J = 1.2$ Hz, 1H), 3.88 (t, $J = 5.4$ Hz, 2H), 3.22–3.35 (m, 1H), 2.92–3.01 (m, 1H), 2.75–2.87 (m, 8H), 2.59–2.70 (m, 2H), 2.45–2.56 (m, 3H), 2.30–2.44 (m, 2H), 1.90–2.00 (m, 2H), 1.66–1.76 (m, 2H).

Resolution of (\pm)-27 by chiral HPLC method 1 gave (–)-27 ($t_{\text{R}} = 6.02$ min) and (+)-27 ($t_{\text{R}} = 7.99$ min). (–)-27: LC-MS (ESI) 435 ($\text{M} + \text{H}$)⁺, $t_{\text{R}} = 4.15$ min, purity 98.0%, method 1. The L-tartaric salt was prepared. $[\alpha]_{\text{D}} = -15.7^\circ$ (c 1.0, EtOH). HRMS (ESI): calcd for $\text{C}_{23}\text{H}_{28}\text{F}_2\text{N}_2\text{O}_2\text{S}$: 434.1839; found: 434.1842. (+)-27: LC-MS (ESI) 435 ($\text{M} + \text{H}$)⁺, $t_{\text{R}} = 4.15$ min, purity 97.0%, method 1. The L-tartaric salt was prepared. $[\alpha]_{\text{D}} = +15.4^\circ$ (c 1.0, EtOH). HRMS (ESI): calcd for $\text{C}_{23}\text{H}_{28}\text{F}_2\text{N}_2\text{O}_2\text{S}$: 434.1839; found: 434.1839.

3-(2'-Fluoro-4',5'-dihydro-1H-spiro[piperidine-4,7'-thieno[2,3-c]pyran]-1-yl) 2-(2-Fluorobenzyl)-N-methyl-N-cyclopropylpropanamide ((\pm)-28). The racemic title compound was prepared from tert-butyl 2-[(2-fluorophenyl)methyl]-3-(2-fluorospiro[4,5-dihydrothieno[2,3-c]pyran-7,4'-piperidine]-1-yl)propanoate¹⁴ (74 mg, 0.15 mmol) and cyclopropyl methylamine hydrochloride (16 mg, 0.15 mmol) according to the general amide formation procedure. The crude product was purified by preparative TLC ($\text{CH}_2\text{Cl}_2/\text{MeOH} = 20:1$) to afford (\pm)-28 (55 mg, 75%) as a white solid.

Resolution of (\pm)-28 by chiral HPLC method 2 (with 0.2% DMEA in hexane/isopropyl alcohol (90:10 v/v) and at 30 mL/min flow rate) gave (–)-28 ($t_{\text{R}} = 6.31$ min) and (+)-28 ($t_{\text{R}} = 7.69$ min). (–)-28: LC-MS (ESI) 461 ($\text{M} + \text{H}$)⁺, 96.58% (UV 214 nm), $t_{\text{R}} = 4.62$ min, purity 99.4%, method 1. ¹H NMR (300 MHz, CDCl_3) δ 7.12–7.17 (m, 2H), 6.94–7.02 (m, 2H), 6.09 (d, $J = 1.8$ Hz, 1H), 3.79–3.89 (m, 3H), 3.03 (dd, $J = 12.9$ Hz, 5.1 Hz, 1H), 2.68–2.79 (m, 7H), 2.45–2.53 (m, 3H), 2.31–2.41 (m, 2H), 2.18–2.21 (m, 1H), 1.91–1.96 (m, 2H), 1.68–1.77 (m, 2H), 0.66–0.80 (m, 3H), 0.33–0.44 (m, 1H). $[\alpha]_{\text{D}} = -14.3^\circ$ (c 0.3, MeOH). HRMS (ESI): calcd for $\text{C}_{25}\text{H}_{31}\text{F}_2\text{N}_2\text{O}_2\text{S} + \text{H}^+$, 461.2069; found, 461.2078.

3-(2'-Fluoro-4',5'-dihydro-1H-spiro[piperidine-4,7'-thieno[2,3-c]pyran]-1-yl) 2-(2-Chlorobenzyl)-N-methyl-N-cyclopropylpropanamide ((\pm)-29). The racemic title compound was prepared from tert-butyl 2-[(2-chlorophenyl)methyl]-3-(2-fluorospiro[4,5-dihydrothieno[2,3-c]pyran-7,4'-piperidine]-1-yl)propanoate¹⁴ (120 mg, 0.25 mmol) and cyclopropyl methylamine hydrochloride (27 mg, 0.25 mmol) according to the general amide formation procedure. The crude product was purified by preparative TLC ($\text{CH}_2\text{Cl}_2/\text{MeOH} = 20:1$) to afford (\pm)-29 (85 mg, 71%) as a white solid.

Resolution of (\pm)-29 by chiral HPLC method 2 (with 0.2% DMEA in hexane/EtOH (90:10 v/v)) gave (–)-29 ($t_{\text{R}} = 5.92$ min) and (+)-29 ($t_{\text{R}} = 7.61$ min). (–)-29: LC-MS (ESI) 477 ($\text{M} + \text{H}$)⁺, $t_{\text{R}} = 4.95$ min, purity 99.4%, method 1. ¹H NMR (300 MHz, CDCl_3) δ 7.33–7.30 (m, 1H), 7.21–7.12 (m, 3H), 6.12 (d, 1H, $J = 1.2$ Hz), 3.99–3.93 (m, 1H), 3.92 (t, 2H, $J = 5.4$ Hz), 3.25 (q, 1H, $J = 4.2$ Hz), 2.85–2.68 (m, 4H), 2.76 (s, 3H), 2.57–2.50 (m, 3H), 2.46–2.32 (m, 2H), 2.05–1.94 (m, 3H), 1.80–1.74 (m, 2H), 0.80–0.61 (m, 3H), 0.28–0.24 (m, 1H). $[\alpha]_{\text{D}} = -43.0^\circ$ (c 0.5, MeOH). HRMS (ESI): calcd for $\text{C}_{25}\text{H}_{31}\text{ClF}_2\text{N}_2\text{O}_2\text{S} + \text{H}^+$, 477.1773; found, 477.1785.

In Vitro NOP Receptor Binding. A filtration-based [³H]-nociceptin binding assay was used to determine the affinity (K_{i}) of synthesized NOP compounds based on previous assay formats,³⁰ with minor modifications. Assay incubations were performed in deep-well 96-well plates with [³H]-nociceptin (final assay concentration 0.2 nM) and 5–10 μg of membrane protein (isolated from CHO cells expressing cloned human NOP receptors) in a final volume of 0.5 mL of HEPES buffer (20 mM; pH 7.4) containing, 5 mM MgCl_2 , 1 mM EDTA, 100 mM NaCl, and 0.1% BSA. Incubations were performed for 60 min at 25 °C and terminated by filtration on glass fiber filtermats (GF/C Filtermat A; pretreated with 0.3% polyethyleneimine for 1 h) on a Tomtec cell harvester. The filters were washed three times with 5 mL of ice-cold Tris-HCl buffer (50 mM, pH 7.4). Filtermats were then dried and embedded with Meltlux scintillant A and the radioactivity counted in a

Microbeta scintillation counter (Perkin-Elmer Life and Analytical Sciences). Specific binding was determined by displacement with 100 nM unlabeled nociceptin. Curves were plotted as the percent of specific inhibition versus NOP compound concentration, and IC_{50} values were determined using four-parameter nonlinear regression routines (XLfit version 4.0, IDBS). K_{i} values were calculated from the IC_{50} by the equation of Cheng and Prusoff,³¹ where $K_{\text{i}} = \text{IC}_{50} \times (1 + D \times K_{\text{d}}^{-1})^{-1}$. Reported values for K_{i} are shown as geometric means \pm the standard error of the mean (SEM), with the number of replicate determinations indicated by n . Geometric means are calculated by the equation $\text{GeoMean} = 10(\text{average}(\log K_{\text{i}1} + \log K_{\text{i}2} + \dots \log K_{\text{i}n})/\text{square root of the number of replicates}, n)$.

In Vitro Opioid Receptor Binding. To determine receptor selectivity to classical opioid receptors, the binding affinity (K_{i}) of NOP compounds was determined in Chinese hamster ovary (CHO) or human embryonic kidney (HEK) 293 cell membranes expressing either cloned human μ , κ , or δ receptors, as previously described.³² Eleven-point ligand displacement curves were determined using [³H]-diprenorphine. Briefly, membranes (4–6 μg protein per reaction) were added to buffer containing 50 mM Tris-HCl, 100 mM NaCl, 1 μM GDP, 5 mM MgCl_2 , and 1 mM EDTA (pH 7.4). The reactions were initiated by the addition of 0.2 nM [³H]-diprenorphine to yield a 500 μL assay volume. The reaction was incubated for 120 min at rt. Specific binding was determined by displacement with 10 μM naltrexone. Reactions were terminated by rapid filtration through glass fiber filters, radioactivity measured and data analyzed using procedures identical to those used for NOP receptor binding.

In Vitro Functional Blockade of NOP Receptor Agonist-mediated G-Protein Activation–GTP γ [³⁵S] Binding. Receptor-mediated G-protein activation can be measured using the non-hydrolyzable radiolabeled analogue of GTP, GTP γ [³⁵S]. Thus, the NOP receptor antagonist affinity (K_{b}) of test ligands was measured in membranes expressing cloned human NOP receptors with a GTP γ [³⁵S] binding assay, according to previously described protocols with minor modifications.^{33,34}

Assays were conducted in deep-well 96-well plates in a 200 μL volume with the following buffer composition: 100 mM NaCl, 20 mM HEPES, 5 mM MgCl_2 , 1 mM EDTA, 0.1% BSA, 3 μM GDP, 0.5 nM GTP γ [³⁵S]. NOP receptor membrane suspension was added at a concentration of 20 μg protein per well, and receptor stimulation was achieved with 300 nM nociceptin. Wheat germ agglutinin-coated scintillation proximity assay (SPA) beads (Perkin-Elmer Life and Analytical Sciences) were added at 1 mg per well to detect membrane-bound GTP γ [³⁵S]. Plates were sealed and incubated for 2 h at rt and then placed at 4 °C overnight to allow the SPA beads to settle. Plates were then counted for radioactivity in a Microbeta Trilux instrument. Specific GTP γ [³⁵S] binding was determined as the difference in cpm observed in the absence and presence of 10 μM unlabeled GTP γ S. Data were plotted as the percent of specific GTP γ [³⁵S] bound from which IC_{50} values were determined using four-parameter nonlinear regression routines (XLfit version 4.0, IDBS). Antagonist affinity (K_{b}) was estimated according to Delapp et al.,³³ using a modification of the equation of Cheng and Prusoff,³¹ where $K_{\text{b}} = \text{IC}_{50} \times (1 + D \times \text{EC}_{50}^{-1})^{-1}$. Reported values for K_{b} are shown as geometric mean \pm the standard error of the mean (SEM), with the number of replicate determinations indicated by n .

Agonist functional GTP γ [³⁵S] binding assays were similar to those described for antagonist measurement, except that the GTP γ [³⁵S] mixture did not have added nociceptin. Basal activity was determined in the absence of added nociceptin. A control nociceptin curve (geometric mean EC_{50} for nociceptin was 2.25 nM, SEM = 0.41, $n = 18$) was included in each assay. The concentration range tested for NOP compounds was 0.17 nM to 10 μM (final assay DMSO concentration in all wells was 1%). The percent efficacy is calculated, relative to nociceptin at 100%.

In Vivo Characterization of Potential tracers in Rat. Doses of potential tracers to be intravenously administered to rats were selected to be low (<10 μg) but still allow accurate detection and quantitation by LC-MS/MS. Thus, each test ligand was dissolved in 25% β -cyclodextrin solution (1 mg/mL) and then diluted to a final ligand

concentration of 6 $\mu\text{g}/\text{mL}$. Each of these solutions was administered intravenously to each of a separate group of three or four rats, injection volume 0.5 mL/kg, via the lateral tail vein. In each group, rats were sacrificed at 10, 20, 40, or 60 min after ligand injection. Samples of hypothalamic, thalamic, and striatal tissue were weighed and placed in conical centrifuge tubes on ice. Four volumes (w/v) of acetonitrile (ACN) containing 0.1% formic acid were added to each tube. These samples were then homogenized using an ultrasonic probe and centrifuged at 14000 rpm for 16 min. Supernatant liquid was diluted by adding sterile water (100–900 μL) in HPLC injection vials for subsequent LC-MS/MS analysis.

Ligands were analyzed with a model 1200 HPLC apparatus (Agilent Technologies, Palo Alto, CA) linked to an API 4000 mass spectrometer (Applied Biosystems, Foster City, CA, USA). A C18 column (2.1 mm \times 50 mm; Agilent; part no. 971700–907) was used for the HPLC. The compound specific isocratic methods consisted of mobile phase of various ratios of water (A) and acetonitrile (B) with 0.1% formic acid. The ratios A/B used were the following: 72/28 ((–)-8), 80/20 ((+)-19), 65/35 ((–)-20), 65/35 ((–)-21), 65/35 ((+)-22), 60/40 ((+)-23), 65/35 ((–)-24), 60/40 ((+)-25), 60/40 ((–)-26), 65/35 ((–)-27), 60/40 ((–)-28), 60/40 ((–)-29), 70/30 ((–)-30), and 60/40 ((–)-33). The ligands were detected by monitoring the precursor to product ion transition. The following are the ion transitions for the compounds listed in Table 5: 389.4 \rightarrow 222.0 ((–)-8), 407.3 \rightarrow 239.9 ((+)-19), 468.5 \rightarrow 256.0 ((–)-20), 454.3 \rightarrow 256.1 ((–)-21), 440.5 \rightarrow 255.9 ((+)-22), 452.2 \rightarrow 257.9 ((+)-23), 438.6 \rightarrow 257.8 ((–)-24), 452.2 \rightarrow 239.9 ((+)-25), 438.3 \rightarrow 240.0 ((–)-26), 435.1 \rightarrow 240.0 ((–)-27), 461.8 \rightarrow 240.3 ((–)-28), 478.3 \rightarrow 240.3 ((–)-29), 421.1 \rightarrow 240.0 ((–)-30), and 463.8 \rightarrow 240.0 ((–)-33). Standards were prepared by adding known quantities of analyte to samples of brain tissue from nontreated rats and processed as described above. The proportion of the injected ligand dose reaching brain region tissue, normalized for animal weight, was expressed as % SUV (standardized uptake value), which was calculated as follows:

$$\% \text{SUV} = \left(\frac{\text{ligand amount measured in tissue (ng/mL)}}{\text{injected ligand dose (}\mu\text{g/kg)}} \right) \times 100$$

Levels of ligand in the hypothalamus,^{16,17} a region with high NOP-1 receptor expression, were taken to represent total ligand binding in a tissue. Thalamus was an intermediate NOP expressing brain region. Striatal levels were used to represent nonspecific binding. It should be noted, however, that striatum^{16,17} does have low NOP-1 receptor expression. Thus, striatum is a pseudo-receptor-null region rather than a true null region. As such, the difference between the ligand concentration measured in the total binding region, the hypothalamus, and that measured in the pseudonull region, the striatum, is an underestimation of the true NOP receptor-specific binding.

To generate the dose occupancy curve, animals were administered an oral dose of 3 or vehicle. One hour following oral pretreatment, animals received an iv dose of unlabeled tracer (–)-27. Forty minutes after the tracer was injected, animals were sacrificed and hypothalamic and striatal tissue were harvested and placed on ice. The procedures outlined above were then applied to the tissue samples collected. Receptor occupancy calculations were made for each animal employing the widely used ratio method.^{12,13}

Computation and Measurement of Lipophilicity. The cLogD values for ligands at pH 7.4 were computed with Pallas 3.7 software (CompuDrug). log *D* values were experimentally determined by the potentiometric method. log *D* values at pH 7.4 were extrapolated from log *P* values determined on a Sirius Analytical GLpKa instrument and Refinement Pro software. Titrations were performed over a defined pH range, with 1-octanol used as the partition solvent.

■ ASSOCIATED CONTENT

● Supporting Information

Experimental and spectroscopic data for compounds 9–18 and HPLC analysis of enantiomerically pure final materials 8, 10,

19–25, and 27–29. This material is available free of charge via the Internet at <http://pubs.acs.org>.

■ AUTHOR INFORMATION

Corresponding Author

*For C.P.: phone, 34-91-6633426; fax, 34-91-6633411; E-mail, conchipe@lilly.com. For V.N.B.: phone, 1-317-433-8151; fax, 1-317-277-0778; E-mail, vparziale@lilly.com.

Notes

The authors declare no competing financial interest.

■ ACKNOWLEDGMENTS

We thank Jiapo Wang, Hao Yao, Heyang Shao, Jinting Tang, Xi Liang, and Zhongzhen Zhang for the preparation of many important compounds. We acknowledge Anju Lewis, Keyue Chen, and Lorrel Burison for the generation of the in vitro binding and functional NOP data and the binding opioid receptor data.

■ ABBREVIATIONS USED

BOC, *tert*-butoxycarbonyl; BBB, blood–brain barrier; BP, binding potential; CNS, central nervous system; DEA, diethylamine; DIPEA, di-isopropylethylamine; DMEA, dimethylethylamine; EDCl, 1-ethyl-3-(dimethylaminopropyl)-carbodiimide; HOBt, 1-hydroxybenzotriazole; LC-MS/MS, liquid chromatography–tandem mass spectrometry; MTBE, methyl *tert*-butyl ether; NCS, *N*-chlorosuccinimide; N/OFQ, nociceptin/orphanin FQ; NOP, nociceptin opioid peptide; ORL1, opioid receptor-like 1; PET, positron emission tomography; RO, receptor occupancy; rt, room temperature; SAR, structure–activity relationship; SPA, scintillation proximity assay; SPECT, single photon emission computed tomography; SUV, standardized uptake value; TLC, thin-layer chromatography; TEA, triethylamine; TFA, trifluoroacetic acid

■ REFERENCES

- (1) Meunier, J. C.; Mollereau, C.; Toll, L.; Suaudeau, C.; Moisand, C.; Alvinerie, P.; Butour, J. L.; Guillemot, J. C.; Ferrara, P.; Monsarrat, B.; Mazarguil, H.; Vassart, G.; Parmentier, M.; Costentin, J. Isolation and structure of the endogenous agonist of opioid-like ORL 1 receptor. *Nature* **1995**, *377*, 532–535.
- (2) Reinschied, R. K.; Nothacker, H.-P.; Bourson, A.; Ardati, A.; Henningsen, R. A.; Bunzow, J. R.; Grandy, D. K.; Langen, H.; Monsma, F., Jr.; Civelli, O. Orphanin FQ: a neuropeptide that activates an opioid-like G-protein coupled receptor. *Science* **1995**, *270*, 792–794.
- (3) Mogli, J. S.; Pasternak, G. W. The molecular and behavioral pharmacology of the orphanin FQ/nociceptin peptide and receptor family. *Pharmacol. Rev.* **2001**, *53*, 381–415.
- (4) Lambert, D. G. The nociceptin/orphanin FQ receptor: a target with broad therapeutic potential. *Nature Rev. Drug Discovery* **2008**, *7*, 694–710.
- (5) Murphy, N. P. The nociceptin/orphanin FQ system as a target for treating alcoholism. *CNS Neurol. Disord.: Drug Targets* **2010**, *9*, 87–93.
- (6) Largent-Milnes, T. M.; Vanderah, T. W. Recently patented and promising ORL-1 ligands: where have we been and where are we going? *Expert Opin. Ther. Pat.* **2010**, *20*, 291–305.
- (7) Phelps, M. E. Positron emission tomography provides molecular imaging of biological processes. *Proc. Natl. Acad. Sci., U.S.A.* **2000**, *97*, 9226–9233.
- (8) Wong, D. F.; Gründer, G.; Brašić, J. R. Brain imaging research: does the science serve clinical practice? *Int. Rev. Ps. Psychiatry* **2007**, *19*, 541–558.

- (9) Lee, C. M.; Farde, L. Using positron emission tomography to facilitate CNS drug development. *Trends Pharmacol. Sci.* **2006**, *27*, 310–316.
- (10) Patel, S.; Gibson, R. In vivo site-directed radiotracers: a mini-review. *Nucl. Med. Biol.* **2008**, *35*, 805–815.
- (11) Pike, V. W. PET Radiotracers: crossing the blood–brain barrier and surviving metabolism. *Trends Pharmacol. Sci.* **2009**, *30*, 431–440.
- (12) Chernet, E.; Martin, L. J.; Li, D.; Need, A. B.; Barth, V. N.; Rash, K. S.; Phebus, L. A. Use of LC/MS to assess brain tracer distribution in preclinical in vivo receptor occupancy studies: Dopamine D2, serotonin 2A and NK-1 receptors as examples. *Life Sci.* **2005**, *78*, 340–346.
- (13) Barth, V. N.; Chernet, E.; Martin, L. J.; Rash, K. S.; Morin, M.; Phebus, L. A. Comparison of rat dopamine D2 receptor occupancy for a series of antipsychotic drugs measured using radiolabeled or unlabeled raclopride tracer. *Life Sci.* **2006**, *78*, 3007–3012.
- (14) Pike, V. W.; Rash, K. S.; Chen, Z.; Pedregal, C.; Statnick, M. A.; Kimura, Y.; Hong, J.; Zoghbi, S. S.; Fujita, M.; Toledo, M. A.; Diaz, N.; Gackenhaimer, S. L.; Tauscher, J. T.; Barth, V. N.; Innis, R. B. Synthesis and Evaluation of Radioligands for Imaging Brain Nociceptin/Orphanin FQ Peptide (NOP) Receptors with Positron Emission Tomography. *J. Med. Chem.* **2011**, *54*, 2687–2700.
- (15) Kimura, Y.; Fujita, M.; Hong, J.; Lohith, T. G.; Gladding, R. L.; Zoghbi, S. S.; Tauscher, J. A.; Goebel, N.; Rash, K. S.; Chen, Z.; Pedregal, C.; Barth, V. N.; Pike, V. W.; Innis, R. B. Brain and Whole-Body Imaging in Rhesus Monkeys of ¹¹C-NOP-1A, a Promising PET Radioligand for Nociceptin/Orphanin FQ Peptide Receptors. *J. Nucl. Med.* **2011**, *52*, 1638–1645.
- (16) Neal, C. R., Jr.; Mansour, A.; Reinscheid, R.; Nothacker, H. P.; Civelli, O.; Akil, H.; Watson, S. J., Jr. Opioid receptor-like (ORL1) receptor distribution in the rat central nervous system: comparison of ORL receptor mRNA expression with ¹²⁵I-(¹⁴Tyr)-orphanin FQ binding. *J. Comp. Neurol.* **1999**, *412*, 563–605.
- (17) Florin, S.; Meunier, J. C.; Costentin, J. Autoradiographic localization of [³H]nociceptin binding sites in the rat brain. *Brain Res.* **2000**, *880*, 11–16.
- (18) Letchworth, S. R.; Mathis, J. P.; Rossi, G. C.; Bodnar, R. J.; Pasternak, G. W. Autoradiographic localization of ¹²⁵I[¹⁴Tyr]orphanin FG/nociceptin and ¹²⁵I[¹⁰Tyr]orphanin FQ/nociceptin(1–11) binding sites in rat brain. *J. Comp. Neurol.* **2000**, *423*, 319–329.
- (19) Bojnik, E.; Farkas, J.; Magyar, A.; Tömböly, C.; Güçlü, U.; Gündüz, O.; Borsodi, A.; Corbani, M.; Benyhe, S. Selective and high affinity labeling of neuronal and recombinant nociceptin receptors with the hexapeptide radioprobe [³H]Ac-RYYRIK-ol. *Neurochem. Int.* **2009**, *55*, 458–466.
- (20) Bridge, K. E.; Wainwright, A.; Reilly, K.; Oliver, K. R. Autoradiographic localization of ¹²⁵I[¹⁴Tyr] nociceptin/orphanin FQ binding sites in macaque primate CNS. *Neuroscience* **2003**, *118*, 513–523.
- (21) Donohue, S. R.; Krushinski, J. H.; Pike, V. W.; Chernet, E.; Phebus, L.; Chesterfield, A. K.; Ferder, C. C.; Halldin, C.; Schaus, J. M. Synthesis, Ex Vivo Evaluation, and Radiolabeling of Potent 1,5-Diphenylpyrrolidin-2-one Cannabinoid Subtype-1 Receptor Ligands as Candidates for In Vivo Imaging. *J. Med. Chem.* **2008**, *51*, 5833–5842.
- (22) Mitch, C. H.; Quimby, S. J.; Diaz, N.; Pedregal, C.; G. de la Torre, M.; Jiménez, A.; Shi, Q.; Canada, E. J.; Kahl, S. D.; Statnick, M. A.; McKinzie, D. L.; Benesh, D. R.; Rash, K. S.; Barth, V. N. Discovery of Aminobenzoyloxyarylamides as κ Opioid Receptor Selective Antagonists: Application to Preclinical Development of a κ Opioid Receptor Antagonist Receptor Occupancy Tracer. *J. Med. Chem.* **2011**, *54*, 8000–8012.
- (23) Ogawa, M.; Hatano, K.; Kawasumi, Y.; Ishiwata, K.; Kawamura, K.; Ozaki, S.; Ito, K. Synthesis and in vivo evaluation of [¹¹C]methyl-Ro-64–6198 as an ORL1 receptor imaging agent. *Nucl. Med. Biol.* **2001**, *28*, 941–947.
- (24) Ogawa, M.; Hatano, K.; Kawasumi, Y.; Wichmann, J.; Ito, K. Synthesis and evaluation of 1-[(3R,4R)-1-cyclooctylmethyl-3-hydroxymethyl-4-piperidyl]-3-[¹¹C]ethyl-1,3-dihydro-2H-benzimidazol-2-one as a brain ORL1 receptor imaging agent for positron emission tomography. *Nucl. Med. Biol.* **2003**, *30*, 51–59.
- (25) Teshima, K.; Minoguchi, M. Remedy for sleep disturbance. Patent WO03082333, 2003.
- (26) Watson, B.; Hohlweg, R.; Thomsen, C. Novel 1,3,8-Triazaspiro Decanones with High Affinity for Opioid Receptor Subtypes. Patent WO 99/59997, 1999.
- (27) Spagnola, B.; Carra, G.; Fantin, M.; Fischetti, C.; Hebbes, C.; McDonald, J.; Barnes, T. A.; Rizzi, A.; Trapella, C.; Fanton, G.; Morari, M.; Lambert, D. G.; Regoli, D.; Calo, G. Pharmacological characterization of the nociceptin/orphanin FQ receptor antagonist SB-612111 [(-)-cis-1-methyl-7-[[4-(2,6-dichlorophenyl)piperidin-1-yl]methyl]-6,7,8,9-tetrahydro-5H-benzocyclohepten-5-ol]: in vitro studies. *J. Pharmacol. Exp. Ther.* **2007**, *321*, 961–967.
- (28) Hirota, M.; Mihara, S.; Nakamura, H.; Koike, H.; Matsumoto, Y. Alpha Aryl or Heteroaryl Methyl Beta Piperidino Propanamide Compounds as ORL1-Receptor Antagonist. Patent WO05092858, 2005.
- (29) Waterhouse, R. N. Determination of lipophilicity and its use as a predictor of blood–brain barrier penetration of molecular imaging agents. *Mol. Imaging Biol.* **2003**, *5*, 376–389.
- (30) Ardati, A.; Henningsen, R. A.; Higelin, J.; Reinscheid, R. K.; Civelli, O.; Monsma, F. J., Jr. Interaction of [³H]orphanin FQ and ¹²⁵I-Tyr14-orphanin FQ with the orphanin FQ receptor: kinetics and modulation by cations and guanine nucleotides. *Mol. Pharmacol.* **1997**, *51*, 816–824.
- (31) Cheng, Y.; Prusoff, W. H. Relationship between constant (K_i) and the concentration of inhibitor which causes 50% inhibition (IC_{50}) of an enzymatic reaction. *Biochem. Pharmacol.* **1973**, *22*, 3099–3108.
- (32) Emmerson, P. J.; McKinzie, J. H.; Surface, P. L.; Suter, T. M.; Mitch, C. H.; Statnick, M. A. Na⁺ modulation, inverse agonism, and anorectic potency of 4-phenylpiperidine opioid antagonists. *Eur. J. Pharmacol.* **2004**, *494* (2–3), 121–130.
- (33) Delapp, N. W.; McKinzie, J. H.; Sawyer, B. D.; Vandergriff, A.; Falcone, J.; McClure, D.; Felder, C. C. Determination of [³⁵S]-guanosine-5'-O-(3-thio)triphosphate binding mediated by cholinergic muscarinic receptors in membranes from Chinese hamster ovary cells and rat striatum using an anti-G protein scintillation proximity assay. *J. Pharmacol. Exp. Ther.* **1999**, *289*, 946–955.
- (34) Ozaki, S.; Kawamoto, H.; Itoh, Y.; Miyaji, M.; Azuma, T.; Ichikawa, D.; Nambu, H.; Iguchi, T.; Iwasawa, Y.; Ohta, H. In vitro and in vivo pharmacological characterization of J-113397, a potent and selective non-peptidyl ORL1 receptor antagonist. *Eur. J. Pharmacol.* **2000**, *402*, 45–53.